OFFICE OF CIVILIAN RADIOACTIVE WASTE MANAGEMENT
DESIGN CALCULATION OR ANALYSIS COVER SHEET

1. QA: QA
2. Page 1

3. System:	4. Document Identifier:	5. Verified:
Uncanistered Spent Nuclear Fuel	000-00C-DSU0-01100-000-00A	☐ Yes ☒ No

6. Title:
Maximum Accelerations on the Fuel Assemblies of a 21-PWR Waste Package during End Impacts

7. Group:
Specialty Analyses and Waste Package Design

8. Document Status Designation:
☒ Preliminary ☐ Final ☐ Superseded ☐ Cancelled

9.

T	F	
☒	☐	1. This product contains no potentially sensitive information.
☐	☒	2. This product contains information that could define a target.
☐	☒	3. This product contains information that could define a specific location.
☐	☒	4. This product contains information that identifies vulnerabilities.

10. Notes/Comments:
N/A

NOTICE OF OPEN CHANGE DOCUMENTS - THIS DOCUMENT IS IMPACTED BY THE LISTED CHANGE DOCUMENTS AND CANNOT BE USED WITHOUT THEM.

---

1) ECN-001, DATED 08/12/2005
2) ECN-002, DATED 08/30/2005

Attachments	Total Number of Pages
See Section 8	

RECORD OF REVISIONS

11. No.	12. Reason for Revision	13. Total No. of Pages	14. Last Page No.	15. Originator (Print/Sign)	16. Checker (Print/Sign)	17. Quality Engineering Representative (Print/Sign)	18. Approved/ Accepted (Print/Sign)	19. Date
A	Initial Issue	66	VII-1	V. de la Brosse V. de la Brosse	S. Mastilovic	W. F. Holub W. F. Holub	M. J. Anderson	3/26/03

CONTENTS

Page

FIGURES

Page

TABLES

Page

1. PURPOSE

The objective of this calculation is to determine the acceleration of the fuel assemblies contained in a 21-Pressurized Water Reactor (PWR) spent nuclear fuel waste package impacting an unyielding surface. A range of initial velocities of the waste package is studied. The scope of this calculation is limited to estimating the acceleration of the fuel assemblies during the impact.

The design of the 21-PWR waste package used in this calculation is that defined in Reference 8. However, a value of 4 *mm* (Ref. 23, Section 8.1.8) was used for the gap between the inner shell (IS) and the outer shell (OS), and the thickness of the OS was reduced by 2 *mm* (See Assumption 3.14). The sketch in Attachment I provides additional information not included in Reference 8. All obtained results are valid for this design only.

This calculation is associated with the waste package design and was performed by the Specialty Analyses and Waste Package Design Section. The waste package (i.e., uncanistered spent nuclear fuel disposal container) is classified as Quality Level 1 (Ref. 13, page 7). Therefore, the preparation of this document is subject to the *Quality Assurance Requirements and Description* (Ref. 16). AP-3.12Q, *Design Calculations and Analyses* (Ref. 25), was used to perform the calculation and develop the document.

2. METHOD

The finite element calculations were performed using the commercially available ANSYS version (V) 5.4 (Ref. 12) and LS-DYNA finite element codes. ANSYS V5.4 was used for preprocessing, i.e., to create a finite element representation (FER) used subsequently in LS-DYNA V950 (Ref. 14) or LS-DYNA V960.1106 (Ref. 10) to obtain solutions. Hereafter, both versions of LS-DYNA will be referred to as "LS-DYNA", unless the distinction is relevant.

The results of these calculations are provided in terms of maximum acceleration of the fuel assemblies. The acceleration time histories presented throughout this document are obtained by two successive differentiation of the corresponding displacement time history. The acceleration unit used throughout this document is *g* (where $g = 9.81$ *m/s* is the acceleration of gravity).

3. ASSUMPTIONS

In the course of developing this document, the following assumptions were made regarding the structural calculations for the waste package. These assumptions do not require confirmation.

3.1 Some of the temperature-dependent material properties are not available for SB-575 N06022 (Alloy 22), SA-240 S31600 (316 stainless steel [SS]), SA-516 K02700 (A 516 Grade 70 carbon steel [CS]), and SA-240 S30400 (304 SS). Therefore, room-temperature (RT) (20 ℃) density and RT Poisson's ratio are assumed for all materials used. The impact of using RT density and RT Poisson's ratio is anticipated to be small. The rationale for this assumption is that these material properties do not change significantly at the temperatures relevant in this calculation and do not have a significant effect on the results. This assumption is used in Section 5.1 and corresponds to paragraph 5.2.8.4 of Reference 20.

3.2 Strain-rate dependent material properties are not available for the materials used. Therefore, the material properties obtained under static loading conditions are assumed for all materials used. In general, this is a conservative assumption; nonetheless, in this case, the impact of using material properties obtained under the static loading conditions is anticipated to be small. The rationale for this assumption is that the mechanical properties of subject materials do not significantly change at the peak strain rates in the course of the end impacts. As presented in Reference 27 (Section 3), the peak strain rate is $50\ s^{-1}$; this strain rate is obtained for an impact speed of $20\ m/s$ (see Ref. 27, Fig. 1), which is bounding for all initial velocities simulated in this document. This assumption is used in Section 5.1 and corresponds to paragraph 5.2.5 of Reference 20.

3.3 The Poisson's ratio of Alloy 22 is not available in literature. Therefore, the Poisson's ratio of Alloy 625 (SB-443 N06625) is assumed for Alloy 22. The impact of this assumption is anticipated to be negligible. The rationale for this assumption is that the chemical compositions of Alloy 22 and Alloy 625 are similar (Ref. 4, Section II, Part B, SB-575, Table 1 and Ref. 2, page 143, respectively). This assumption is used in Section 5.1.1 and corresponds to paragraph 5.2.8.2 of Reference 20.

3.4 The uniform strain of Alloy 22 and 316 SS are not available in literature. Therefore it is conservatively assumed that the uniform strain is 90% of the elongation. The rationale for this assumption is the character of the stress-strain curve for Alloy 22 and 316 SS (Ref. 19 and Ref. 7, page 304, respectively). This assumption is used in Section 5.1.2 and corresponds to paragraph 5.2.8.6 of Reference 20.

3.5 The uniform strain of 304 SS is not available in literature. Therefore it is conservatively assumed that the uniform strain is 75% of the elongation. The rationale for this assumption is the character of the stress-strain curve for 304 SS (Ref. 7, page 295). This assumption is used in Section 5.1.2 and corresponds to paragraph 5.2.14.1 of Reference 20.

3.6 The uniform strain of A 516 Grade 70 CS is not available in literature. Therefore it is conservatively assumed that the uniform strain is 50% of the elongation. The rationale for this assumption is the character of the stress-strain curve for A 36 CS (Ref. 7, page 189) that has similar chemical composition to A 516 Grade 70 CS (see Ref. 4, Section II, Part A, SA-516/SA-516M, Table 1 and SA-36/SA-36M, Table 2 for chemical compositions of A 516 Grade 70 CS and A 36 CS, respectively). This assumption is used in Section 5.1.2 and corresponds to paragraph 5.2.11.1 of Reference 20.

3.7 The change of minimum elongation with increase of temperature for 316 SS is not available in literature. Therefore, the magnitude of this change at elevated temperature is assumed, based on the relative change of typical elongation for said materials available in vendor catalogues (Ref. 1, page 8). The rationale for this assumption is that the relative change of typical elongation should be bounding for the relative change of minimum elongation. This assumption is used in Section 5.1.1 and corresponds to paragraph 5.2.8.5 of Reference 20.

3.8 The exact geometry of the PWR fuel assemblies is simplified for the purpose of this calculation in such a way that its total mass is assumed to be distributed within a bar of square cross section with uniform mass density. The rationale for this assumption is to provide a set of bounding results, while simplifying the FER. This assumption is used in Section 5.3.1 and corresponds to paragraph 5.2.9.1 of Reference 20.

3.9 The material used to represent the fuel assemblies is 304 SS. The rationale for this assumption is that the end fittings of the fuel assemblies are made of 304 SS (Ref. 24, Section 2.1, page 2-4) and they are the parts that will come in contact with other components. This assumption is used in Sections 5.1.1 and 5.3.1 and corresponds to paragraph 5.2.9.2 of Reference 20.

3.10 The following design parameters are assumed for the PWR spent nuclear fuel assemblies to be loaded into a 21-PWR waste package: mass = 773.4 *kg*, width = 216.9 *mm*, and length = 4407 *mm*. The rationale for this assumption is that these parameters correspond to the B&W (Babcock & Wilcox) 15x15 fuel assembly, which is the heaviest PWR fuel assembly available (Ref. 9, Table 2). The mass of the B&W fuel assembly has been increased by 25 *lbs* (11.4 *kg*) to account for variations in fuel assembly mass. It should be noted that South Texas PWR fuel assemblies will not be disposed in the 21-PWR waste package, and are therefore excluded from this assumption. This assumption is used in Section 5.3.1 and corresponds to paragraph 5.2.9.5 of Reference 20.

3.11 The target surface was assumed to be unyielding (i.e., elastic), and A 36 CS was used to represent it in the FER. The rationale for this assumption was that this material has a high modulus of elasticity compared to concrete and it is known that the use of an unyielding surface with high modulus of elasticity would ensure conservative results in terms of stresses in the waste package. This assumption is used in Section 5.1.1 and 5.3.1 and corresponds to paragraph 5.2.8.1 of Reference 20.

3.12 The friction coefficients for contacts occurring between the materials used in this calculation are not available in literature. It is, therefore, assumed that the dynamic (sliding) friction coefficient is 0.5 for all contacts. The rationale for this assumption is that this friction coefficient represents the reasonable typical value for most metal-on-metal contacts (see Ref. 6, Table 3.2.1, page 3-26). This assumption is used in Section 5.3.1.

3.13 The variation of functional friction coefficient between the static and dynamic value as a function of relative velocity of the surfaces in contact (see Ref. 18, page 6.9) is not available in literature for the materials used in this calculation. Therefore, the effect of relative velocity of the surfaces in contact is neglected in this calculation by assuming that the functional friction coefficient and static friction coefficient are both equal to the dynamic friction coefficient. The impact of this assumption on results presented in this document is anticipated to be negligible. The rationale for this conservative assumption is that it provides a bounding set of results by minimizing the friction coefficient within the given finite element analysis framework. This assumption is used in Section 5.3.1 and corresponds to paragraph 5.2.14.4 of Reference 20.

3.14 The thickness of the WP OS is reduced by 2 *mm*. The rationale for this assumption is the following: The OS will degrade due to general corrosion during the regulatory period. The thickness reduction of 2 mm over the regulatory period of 10,000 years corresponds to a general corrosion rate of $2 \cdot 10^{-4}$ *mm/yr*. According to Reference 22 (See file WDgA22Sand_all), the general corrosion rate of $2 \cdot 10^{-4}$ *mm/yr* exceeds the 97th percentile of general corrosion rate for Alloy 22. This assumption is used in Sections 1 and 5.3.1.

4. USE OF COMPUTER SOFTWARE

One of the finite element analysis (FEA) computer codes used for this calculation is ANSYS V5.4 (Ref. 12), which was obtained from Software Configuration Management in accordance with appropriate procedures, and is identified by the Computer Software Configuration Item number 30040 V5.4. ANSYS V5.4 is a qualified, commercially available FEA code and is appropriate for creating a mesh as performed in this calculation. The calculations using the ANSYS V5.4 software were executed on the Hewlett-Packard (HP) 9000 series UNIX workstation (operating system HP-UX B.10.20) identified with YMP (Yucca Mountain Project) tag number 117162 located in Las Vegas, Nevada. The ANSYS evaluation performed for this calculation is fully within the range of the validation performed for the ANSYS V5.4 code. Access to the code was granted by the Software Configuration Management in accordance with the appropriate procedures.

The input files (identified by .inp file extensions) and output files (identified by .out file extensions) for ANSYS V5.4 are provided in Attachment VIII.

The other FEA computer code used for this calculation is Livermore Software Technology Corporation LS-DYNA (V950 [Ref. 14] and V960.1106 [Ref. 10]), which was obtained from the Software Configuration Management in accordance with appropriate procedures. These two versions of LS-DYNA are identified by the Software Tracking Numbers 10300-950-00 and 10300-960.1106-00, respectively. LS-DYNA is a qualified, commercially available FEA code and both versions are appropriate for structural calculations of waste packages as performed in this calculation. These two versions of the LS-DYNA code perform the same way for the simulations run in this calculation, and both versions were used in order to take advantage of all the available computing resources. The calculations using LS-DYNA V950 were executed on the HP 9000 series UNIX workstations (operating system HP-UX B.10.20) identified with YMP tag number 117162 and 117161 located in Las Vegas, Nevada. The calculations using LS-DYNA V960.1106 were executed on the HP 9000 series UNIX workstation (operating system HP-UX 11.0) identified with YMP tag number 151325 and 150691 located in Las Vegas, Nevada. The LS-DYNA evaluations performed for this calculation are fully within the range of the validation performed for both versions of the LS-DYNA code. Access to the code was granted by the Software Configuration Management in accordance with the appropriate procedures.

The input files (identified by .k and .inc file extensions) and output files (filenames "d3hsp") for LS-DYNA are provided in Attachment VIII.

The results obtained in LS-DYNA are post-processed using LSPOST V2 (Livermore Software Technology Corporation), which is a graphical representation plotting tool exempt in accordance with Reference 26 (Section 2.1.2).

The average peak accelerations (see Table 5) are calculated using the commercial off-the-shelf software Microsoft® Excel 97 SR-2. These calculated values can be checked by hand. Thus, Microsoft® Excel is an exempt software according to Reference 26 (Section 2.1.1).

5. CALCULATION

5.1 MATERIAL PROPERTIES

Material properties used in this calculation are listed in this section. Some of the temperature-dependent material properties are not available for the materials used in this calculation. Therefore, RT density and RT Poisson's ratio are used for all materials (see Assumption 3.1). Furthermore, all material properties listed below were obtained under static loading conditions (see Assumption 3.2).

The values of each material property are needed at 150 ℃ (302 ℉) and 200 ℃ (392 ℉). The material properties at these temperatures are obtained by linear interpolation of the corresponding material properties presented in Table 1, by using the formula:

$$p = p(T) = p_l + \left(\frac{T - T_l}{T_u - T_l}\right) \cdot (p_u - p_l)$$

Subscripts u and l denote the upper and lower bounding values of generic material property p at the corresponding bounding temperatures.

Table 1. Material Properties Cited in References

		Temperature (℃ - ℉)	Value	Reference
Alloy 22	Yield Strength	93 - 200	338 *MPa*	Ref. 21, Values for Plates, ¼ - ¾ in. (6.4 – 19.1 mm) thick
		204 - 400	283 *MPa*	
	Tensile Strength	93 - 200	738 *MPa*	Ref. 21, Values for Plates, ¼ - ¾ in. (6.4 – 19.1 mm) thick
		204 - 400	676 *MPa*	
	Elongation	93 - 200	65 %	Ref. 21, Values for Plates, ¼ - ¾ in. (6.4 – 19.1 mm) thick
		204 - 400	66 %	
	Modulus of Elasticity	93 - 200	203 *GPa*	Ref. 21, Values for Sheets, 0.028 – 0.125 in. (0.713-3.2 mm) thick
		204 - 400	196 *GPa*	

		Temperature (°C - °F)	Value	Reference
316 SS	**Yield Strength**	93 - 200	25.9 *ksi*	Ref. 4, Section II, Part D, Table Y-1
		121 - 250	24.6 *ksi*	
		149 - 300	23.4 *ksi*	
		204 - 400	21.4 ksi	
	Tensile Strength	93 - 200	75.0 *ksi*	Ref. 4, Section II, Part D, Table U
		149 - 300	72.9 *ksi*	
		204 - 400	71.9 *ksi*	
	Typical Elongation	93 - 200	54.0 %	Ref. 1, page 8
		204 - 400	51.0 %	
	Modulus of Elasticity	93 - 200	27.6 e6 *psi*	Ref. 4, Section II, Part D, Table TM-1
		149 - 300	27.0 e6 *psi*	
		204 - 400	26.5 e6 *psi*	
304 SS	**Yield Strength**	93 - 200	25.0 *ksi*	Ref. 4, Section II, Part D, Table Y-1
		121 - 250	23.6 *ksi*	
		149 - 300	22.4 *ksi*	
		204 - 400	20.7 ksi	
	Tensile Strength	93 - 200	71.0 *ksi*	Ref. 4, Section II, Part D, Table U
		149 - 300	66.2 *ksi*	
		204 - 400	64.0 *ksi*	
	Modulus of Elasticity	93 - 200	27.6 e6 *psi*	Ref. 4, Section II, Part D, Table TM-1
		149 - 300	27.0 e6 *psi*	
		204 - 400	26.5 e6 *psi*	

		Temperature (°C - °F)	Value	Reference
516 CS	Yield Strength	93 - 200	34.8 *ksi*	Ref. 4, Section II, Part D, Table Y-1
		121 - 250	34.2 *ksi*	
		149 - 300	33.6 *ksi*	
		204 - 400	32.5 ksi	
	Tensile Strength	93 - 200	70.0 *ksi*	Ref. 4, Section II, Part D, Table U
		149 - 300	70.0 *ksi*	
		204 - 400	70.0 *ksi*	
	Modulus of Elasticity	93 - 200	28.8 e6 *psi*	Ref. 4, Section II, Part D, Table TM-1
		149 - 300	28.3 e6 *psi*	
		204 - 400	27.7 e6 *psi*	

5.1.1 Material properties at 150 °C and 200 °C

SB-575 N06022 (Alloy 22) (OS, OS lids, extended OS lid, upper and lower trunnion collar sleeves, and inner shell support ring):

- Density = 8690 kg/m^3 (0.314 lb/in^3) (at RT) (Ref. 21, Paragraph "Properties of Alloy 22")
- Yield strength = 310 *MPa* at 150 °C
  Yield strength = 285 *MPa* at 200 °C
- Tensile strength = 706 *MPa* at 150 °C
  Tensile strength = 678 *MPa* at 200 °C
- Elongation = 0.66 at 150 °C
  Elongation = 0.66 at 200 °C
- Poisson's ratio = 0.278 (at RT) (Ref. 21, paragraph "Mechanical Properties"; See Assumption 3.3)
- Modulus of elasticity = 199 *GPa* at 150 °C
  Modulus of elasticity = 196 *GPa* at 200 °C

SA-240 S31600 (316 SS) (inner shell, inner shell lids, shear ring and shell interface ring):

- Density = 7980 kg/m^3 (at RT) (Ref. 5, Table X1.1, p. 7)

- Yield strength = 161 *MPa* (23.4 *ksi*) at 150 ℃
  Yield strength = 149 *MPa* (21.6 *ksi*) at 200 ℃

- Tensile strength = 503 *MPa* (72.9 *ksi*) at 150 ℃
  Tensile strength = 496 *MPa* (72.0 *ksi*) at 200 ℃

- Minimum elongation = 0.40 (at RT) (Ref. 4, Section II, Part A, SA-240, Table 2).
  The change of minimum elongation with increase of temperature for 316 SS is not available in literature. Therefore, the magnitude of this change is estimated based on the relative change of typical elongation (see Assumption 3.7 and Ref. 1) and applied to the value of the minimum elongation at RT (see Table 2).

Table 2. Change in Typical Elongation for 316 SS between RT and High Temperatures

Temperature (°C)	RT	150	200
Typical Elongation (%)	0.68	0.525	0.511
Change in Typical Elongation between RT and Higher Temperature (%)	N/A	-23	-25

Minimum elongation for 316 SS at 150 ℃: 0.4 · (1-0.23) = 0.31
Minimum elongation for 316 SS at 200 ℃: 0.4 · (1-0.25) = 0.30

- Poisson's ratio = 0.30 (at RT) (Ref. 2, Figure 15, p. 755)

- Modulus of elasticity = 186 *GPa* ($27.0 \cdot 10^6$ *psi*) at 150 ℃
  Modulus of elasticity = 183 *GPa* ($26.6 \cdot 10^6$ *psi*) at 200 ℃

SA-240 S30400 (304 SS) (PWR fuel assemblies, see Assumption 3.9):

- Yield strength = 154 *MPa* (22.4 *ksi*) at 150 ℃
  Yield strength = 143 *MPa* (20.8 *ksi*) at 200 ℃

- Tensile strength = 456 *MPa* (66.2 *ksi*) at 150 ℃
  Tensile strength = 443 *MPa* (64.2 *ksi*) at 200 ℃

- Elongation = 0.40 (at RT) (Ref. 4, Section II, Part A, SA-240, Table 2)

- Poisson's ratio = 0.29 (at RT) (Ref. 2, Figure 15, p. 755)

- Modulus of elasticity = 186 *GPa* ($27.0 \cdot 10^6$ *psi*) at 150 ℃
  Modulus of elasticity = 183 *GPa* ($26.6 \cdot 10^6$ *psi*) at 200 ℃

SA-516 K02700 (A 516 Grade 70 CS) (basket guides and stiffeners, fuel basket plates and tubes):

- Density = 7850 kg/m^3 (at RT) (Ref. 4, Section II, Part A, SA-20/SA-20M, Section 14.1) (Material supplied to American Society for Testing and Materials [ASTM] A 516/A 516M-90 specification shall conform to specification ASTM A 20/A 20M [see Ref. 4, Section II, Part A, SA-516/SA-516M, Section 3.1])

- Yield strength = 232 *MPa* (33.6 *ksi*) at 150 ℃
  Yield strength = 225 *MPa* (32.6 *ksi*) at 200 ℃

- Tensile strength = 483 *MPa* (70 *ksi*) at 150 ℃
  Tensile strength = 483 *MPa* (70 *ksi*) at 200 ℃

- Elongation = 0.21 (at RT) (Ref. 4, Section II, Part A, SA-516/SA-516M, Table 2)

- Poisson's ratio = 0.3 (at RT) (Ref. 3, p. 374)

- Modulus of elasticity = 195 *GPa* ($28.3 \cdot 10^6$ *psi*) at 150 ℃
  Modulus of elasticity = 191 *GPa* ($27.7 \cdot 10^6$ *psi*) at 200 ℃

SA-36 K02600 (A 36 CS) (unyielding surface, see Assumption 3.11):

- Density = 7860 kg/m^3 (at RT) (Ref. 5, Table X1.1, p. 7)

- Poisson's ratio = 0.30 (at RT) (Ref. 3, p. 374)

- Modulus of elasticity = 203 *GPa* ($29.5 \cdot 10^6$ *psi*) (at RT) (Ref. 4, Section II, Part D, Table TM-1)

5.1.2 Calculations for True Measures of Ductility

The material properties in Section 5.1 refer to engineering stress and strain definitions: $s = P/A_0$ and $e = L/L_0 - 1$, where P stands for the force applied during static tensile test, L is the deformed-specimen length, and L_0 and A_0 are original length and cross-sectional area of specimen, respectively. The engineering stress-strain curve does not give a true indication of the deformation characteristics of a material during plastic deformation since it is based entirely on the original dimensions of the specimen. In addition, ductile metal that is pulled in tension becomes unstable and necks down during the test. Hence, LS-DYNA FEA code requires input in terms of true stress and strain definition: $\sigma = P/A$ and $\varepsilon = \ln (L/L_0)$ (see Ref. 15, Chapter 9).

The relationships between the true stress and strain definitions and engineering stress and strain definitions, $\sigma = s(1+e)$ and $\varepsilon = \ln(1+e)$ (see Ref. 15, Chapter 9), can be readily derived based on constancy of volume ($A_0 \cdot L_0 = A \cdot L$) and strain homogeneity during plastic deformation. These expressions are applicable only in the hardening region of stress-strain curve that is limited by the onset of necking.

The following parameters are used in the subsequent calculations:

$s_y \approx \sigma_y$ = yield strength

s_u = engineering tensile strength

σ_u = true tensile strength

$e_y \approx \varepsilon_y$ = strain corresponding to yield strength ($=\frac{\sigma_y}{E}$)

E = modulus of elasticity

e_u = engineering strain corresponding to tensile strength (engineering uniform strain)

ε_u = true strain corresponding to tensile strength (true uniform strain)

In the absence of uniform strain data in available literature, it needs to be estimated based on the character of stress-strain curves and elongation (strain corresponding to rupture of the tensile specimen).

The stress-strain curves for Alloy 22 and 316 SS do not manifest pronounced softening phase (see Ref. 19 and Ref. 7, page 304). Therefore, the elongation, reduced by 10% to take into account the specimen-failure part of the stress-strain curve (see Assumption 3.4), can be used in place of uniform strain for these two materials.

For Alloy 22:

$e_u = 0.9 \cdot elongation = 0.9 \cdot 0.66 = 0.59$, $\varepsilon_u = \ln(1+0.59) = 0.46$ and
$\sigma_u = 706 \cdot (1+0.59) = 1120\ MPa$ at 150 ℃
$e_u = 0.9 \cdot 0.66 = 0.59$, $\varepsilon_u = \ln(1+0.59) = 0.46$ and $\sigma_u = 678 \cdot (1+0.59) = 1080\ MPa$ at 200 ℃

For 316 SS:

$e_u = 0.9 \cdot 0.4 \cdot (1-0.23) = 0.28$, $\varepsilon_u = \ln(1+0.28) = 0.25$ and $\sigma_u = 503 \cdot (1+0.28) = 644\ MPa$ at 150 ℃
$e_u = 0.9 \cdot 0.4 \cdot (1-0.25) = 0.27$, $\varepsilon_u = \ln(1+0.27) = 0.24$ and $\sigma_u = 496 \cdot (1+0.27) = 630\ MPa$ at 200 ℃

Contrary to the two previous cases, the stress-strain curve for 304 SS exhibits pronounced three-stage (elastic-hardening-softening) deformation character. The uniform strain is, therefore, estimated to be 75% of elongation based on the available stress-strain curves (see Assumption 3.5).

Hence $e_u = 0.75 \cdot \text{elongation} = 0.75 \cdot 0.40 = 0.30$. The true uniform strain is therefore

$$\varepsilon_u = \ln(1 + e_u) = \ln(1 + 0.30) = 0.26$$

The true tensile strength is

$$\sigma_u = s_u \cdot (1 + e_u) = 456 \cdot (1 + 0.30) = 593\,MPa \text{ (at } 150\,℃)$$
$$\sigma_u = s_u \cdot (1 + e_u) = 443 \cdot (1 + 0.30) = 576\,MPa \text{ (at } 200\,℃)$$

Finally, the stress-strain curve for A 516 Grade 70 CS exhibits stress-strain curve character typical for CS. The uniform strain is estimated to be 50 % of elongation based on the available stress-strain curves for A 36 CS (see Assumption 3.6).

Hence $e_u = 0.5 \cdot \text{elongation} = 0.5 \cdot 0.21 = 0.11$. The true uniform strain is therefore

$$\varepsilon_u = \ln(1 + e_u) = \ln(1 + 0.11) = 0.10$$

Since the engineering tensile strength of A 516 Grade 70 CS does not vary with temperature for the temperature range of interest, the true tensile strength is

$$\sigma_u = s_u \cdot (1 + e_u) = 483 \cdot (1 + 0.11) = 536\,MPa \text{ (at } 150\,℃ \text{ and at } 200\,℃)$$

5.1.3 Calculations for Tangent Moduli

As previously discussed, the results of this simulation are required to include elastic and plastic deformations for Alloy 22, 316 SS, A 516 Grade 70 CS, and 304 SS. When the materials are driven into the plastic range, the slope of stress-strain curve continuously changes. A ductile failure is preceded by a protracted regime of hardening (and possibly softening) and substantial accumulation of inelastic strains. Thus, a simplification for this curve was needed to incorporate plasticity into the FER. A standard approximation (commonly used in engineering) is to use a straight line that connects the yield point and the ultimate tensile strength point of the material. The tangent modulus (E_t) is a parameter used in the subsequent calculations in addition to those defined in Section 5.1. The tangent modulus represents the slope of the stress-strain curve in the plastic region; it can be calculated using the following expression:

$$E_t = (\sigma_u - \sigma_y)/(\varepsilon_u - \sigma_y/E)$$

and the material properties given in Sections 5.1.1 and 5.1.2. For example, for Alloy 22 at 150 ℃, $E_t = (1.12 - 0.310) / (0.46 - 310 \cdot 10^6 / 199 \cdot 10^9) = 1.77$ *GPa*. The values of tangent moduli used in this calculation are presented in Table 3.

Table 3. Tangent Moduli at Two Different Temperatures

Material	Tangent Modulus (GPa)	
	150 ℃	200 ℃
Alloy 22	1.77	1.73
316 SS	1.94	2.02
304 SS	1.69	1.67
A 516 CS	3.08	3.15

5.2 INITIAL CONDITIONS FOR THE DROPS

The initial velocities for the impacts are 0.5, 1, 2, 4 and 6 *m/s*. The angle between the axis of the waste package and the vertical (α, see Figure 1) is 1 *degree*.

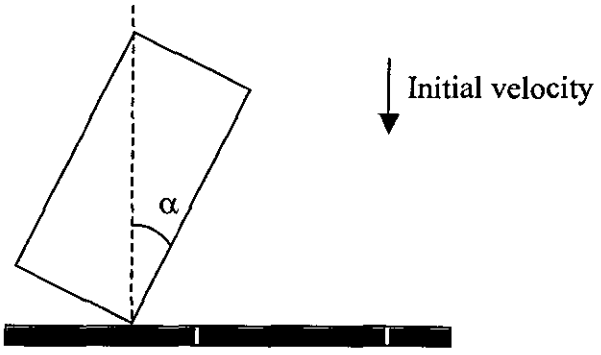

Figure 1. Initial Position of the Waste Package for the End Impacts

5.3 FINITE ELEMENT REPRESENTATION

5.3.1 Description of the Finite Element Representation

A half-symmetry, three-dimensional FER of the waste package is developed in ANSYS V5.4 using the dimensions provided in Attachment I. The internal structure of the waste package is simplified in several ways. The PWR fuel assemblies are reduced to bars of square cross section of uniform mass density, and assumed to be constructed of 304 SS (Assumptions 3.8 and 3.9). Also, the geometric dimensions of the fuel assemblies are modified to keep the value of the gap between the

fuel assemblies and the nearest element consistent with the gap defined using the elements found in Attachment I and Assumption 3.10. Furthermore, the fuel basket tubes and fuel basket plates are not represented in the FER. Finally, the mass density of the basket stiffeners is modified so that the total mass of the loaded waste package equals the mass given in Attachment I.

The thickness of the OS is reduced by 2 mm on its outer surface (see Assumption 3.14). The radial gap between the IS and the OS is 4 *mm* (see Section 1).

The target surface is conservatively assumed to be unyielding and made of A 36 CS (Assumption 3.11).

A friction coefficient of 0.5 is used between all parts in contact (Assumptions 3.12 and 3.13).

Neither system damping nor contact damping are applied during the impact simulation.

5.3.2 Initial Gap between the Fuel Assemblies and the IS Bottom Lid

The kinematics of the problem may vary with the initial gap between the fuel assemblies and the IS bottom lid, which may affect the acceleration of the fuel assemblies. In order to ensure that the maximum acceleration in the fuel assemblies is reached, the value to give this gap is studied in Attachment II. It shows that the configuration where the initial gap between the fuel assemblies and the IS bottom lid is minimum yields the highest maximum acceleration. This configuration is used for all results presented in the document.

5.3.3 Mesh Objectivity

The mesh of the FER is generated and refined in the contact region according to standard engineering practice. This mesh is then further refined in the region of contact (fuel assemblies and IS bottom lid) to verify that the results are not mesh-sensitive. The variation in volume of a representative element and the variation in acceleration experienced by the fuel assemblies are compared, according to the method described in Reference 20, Section 6.2.3. The results are presented in Attachment III. Since the criterion defined in Reference 20, Section 6.2.3, is met, the accuracy and representativeness of the mesh are deemed acceptable for this calculation.

5.3.4 Output Period for the Results

During the simulations, the results are recorded at a frequency defined by the user. The frequency at which the results are recorded must be high enough to capture the maximum value of accelerations. Attachment IV shows that for this simulation, an output period of 0.0001 *s* ensures the stability of the results. This output period is then used for all results presented in this document.

6. RESULTS

The FER described in Section 5.3 is used to run the simulations corresponding to the initial conditions listed in Section 5.2. Table 4 presents the maximum peak acceleration (in the axial direction of the fuel assemblies) experienced by the fuel assemblies during each simulation at 150 ℃. Table 5 presents the average peak acceleration for each impact. The average peak acceleration is obtained by calculating the average peak value of all curves presented in the corresponding figure (see Attachment V for details). Butterworth filter is used (with three different cutoff frequencies) to remove the high frequency response for all the results presented in this document. The choice of cutoff frequencies is elaborated in Attachment VII.

Table 4. Maximum Peak Acceleration (*g*) for the Fuel Assemblies with Three Different Cutoff Frequencies

	Initial Velocity (*m/s*)				
Cutoff Frequency (*Hz*)	**0.5**	**1**	**2**	**4**	**6**
450	75 (See Figure V- 1)	144 (See Figure V- 4)	263 (See Figure V- 7)	323 (See Figure V- 10)	506 (See Figure V- 13)
600	101 (See Figure V- 2)	192 (See Figure V- 5)	347 (See Figure V- 8)	369 (See Figure V- 11)	567 (See Figure V- 14)
1000	136 (See Figure V- 3)	343 (See Figure V- 6)	502 (See Figure V- 9)	479 (See Figure V- 12)	701 (See Figure V- 15)

Table 5. Average Peak Acceleration (*g*) for the Fuel Assemblies with Three Different Cutoff Frequencies

	Initial Velocity (*m/s*)				
Cutoff Frequency (*Hz*)	**0.5**	**1**	**2**	**4**	**6**
450	35 (Corresponds to Figure V- 1)	72 (Corresponds to Figure V- 4)	115 (Corresponds to Figure V- 7)	155 (Corresponds to Figure V- 10)	194 (Corresponds to Figure V- 13)
600	48 (Corresponds to Figure V- 2)	99 (Corresponds to Figure V- 5)	147 (Corresponds to Figure V- 8)	180 (Corresponds to Figure V- 11)	219 (Corresponds to Figure V- 14)
1000	78 (Corresponds to Figure V- 3)	160 (Corresponds to Figure V- 6)	215 (Corresponds to Figure V- 9)	244 (Corresponds to Figure V- 12)	278 (Corresponds to Figure V- 15)

In addition, two cases were run at 200 ℃, the first with an initial velocity of 1 *m/s* and the second with an initial velocity of 4 *m/s*. The results obtained are presented in Attachment VI. The variation of temperature of 50 ℃ has minor effect on the results.

Originator: VB. March 25,03 Checker: 25 March 2003

The output values are reasonable for the given inputs in this calculation. The uncertainties are taken into account by varying the most important parameters such as initial velocity and cutoff frequency. The results are suitable for use in assessing the acceleration on the fuel assemblies due to the impact of the waste package on an unyielding surface.

7. REFERENCES

1. Allegheny Ludlum 1999. "Technical Data Blue Sheet, Stainless Steels, Chromium-Nickel-Molybdenum, Types 316 (S31600), 316L (S31603), 317 (S31700), 317L (S31703)." Pittsburgh, Pennsylvania: Allegheny Ludlum Corporation. Accessed July 31, 2000. TIC: 248631. http://www.alleghenytechnologies.com/ludlum/pages/products/t316_317.pdf

2. ASM (American Society for Metals) 1980. *Properties and Selection: Stainless Steels, Tool Materials and Special-Purpose Metals.* Volume 3 of *Metals Handbook.* 9th Edition. Benjamin, D., ed. Metals Park, Ohio: American Society for Metals. TIC: 209801.

3. ASM International 1990. *Properties and Selection: Irons, Steels, and High-Performance Alloys.* Volume 1 of *Metals Handbook* 10th Edition. Materials Park, Ohio: ASM International. TIC: 245666.

4. ASME (American Society of Mechanical Engineers) 2001. *2001 ASME Boiler and Pressure Vessel Code (includes 2002 addenda).* New York, New York: American Society of Mechanical Engineers. TIC: 251425

5. ASTM G 1-90 (Reapproved 1999). 1999. *Standard Practice for Preparing, Cleaning, and Evaluating Corrosion Test Specimens.* West Conshohocken, Pennsylvania: American Society for Testing and Materials. TIC: 238771.

6. Avallone, E.A. and Baumeister, T., III, eds. 1987. Marks' Standard Handbook for Mechanical Engineers. 9th Edition. New York, New York: McGraw-Hill. TIC: 206891.

7. Boyer, H.E., ed. 2000. *Atlas of Stress-Strain Curves.* Metals Park, Ohio: ASM International. TIC: 248901.

8. BSC (Bechtel SAIC Company) 2001. *Repository Design, Waste Package, Project 21-PWR Waste Package with Absorber Plates, Sheet 1 of 3, Sheet 2 of 3, and Sheet 3 of 3.* DWG-UDC-ME-000001 REV A. Las Vegas, Nevada: Bechtel SAIC Company. ACC: MOL.20020102.0174.

9. BSC (Bechtel SAIC Company) 2001. *Uncanistered Spent Nuclear Fuel Disposal Container System Description Document* SDD-UDC-SE-000001 REV 01 ICN 01 Las Vegas, Nevada: Bechtel SAIC Company ACC: MOL.20010927.0070.

10. BSC (Bechtel SAIC Company) 2002. *Software Code: LS-DYNA.* V960.1106. HP9000. 10300-960.1106-00.

11. CRWMS M&O 1997. *Waste Container Cavity Size Determination.* BBAA00000-01717-0200-00026 REV 00. Las Vegas, Nevada: CRWMS M&O. ACC: MOL.19980106.0061.

12. CRWMS M&O 1998. *ANSYS.* V5.4. HP-UX 10.20. 30040 5.4.

13. CRWMS M&O 1999. *Classification of the MGR Uncanistered Spent Nuclear Fuel Disposal Container System.* ANL-UDC-SE-000001 REV 00. Las Vegas, Nevada: CRWMS M&O. ACC: MOL.19990928.0216.

14. CRWMS M&O 2000. *Software Code: LS-DYNA.* V950. HP 9000. 10300-950-00.

15. Dieter, G.E. 1976. *Mechanical Metallurgy.* 2nd Edition. Materials Science and Engineering Series. New York, New York: McGraw-Hill Book Company. TIC: 247879.

16. DOE (U.S. Department of Energy) 2002. *Quality Assurance Requirements and Description.* DOE/RW-0333P, Rev. 12. Washington, D.C.: U.S. Department of Energy, Office of Civilian Radioactive Waste Management. ACC: MOL.20020819.0387.

17. Stokey, W.F. 1996. "Vibration of Systems Having Distributed Mass and Elasticity." Chapter 7 of *Shock and Vibration Handbook.* 4th Edition. Harris, C.M., ed. New York, New York: McGraw-Hill. TIC: 241055.

18. Livermore Software Technology Corporation 2001. LS-DYNA Keyword User's Manual, Version 960. Livermore, California: Livermore Software Technology Corporation. TIC: 252119.

19. LL020603612251.015. Slow Strain Rate Test Generated Stress Corrosion Cracking Data. Submittal date: 08/27/2002.

20. McKenzie, D.G., IV. 2002. *Waste Package Design Methodology Report.* TDR-MGR-MD-000006 REV 02. Las Vegas, Nevada: Bechtel SAIC Company. ACC: MOL.20020404.0085.

21. MO0003RIB00071.000. Physical and Chemical Characteristics of Alloy 22. Submittal date: 03/13/2000.

22. MO0010SPASIL02.002. Silica Adjusted General Corrosion Rates of Alloy 22 and Titanium Grade 7. Submittal date: 10/10/2000.

23. Plinski, M.J. 2001. *Waste Package Operations Fabrication Process Report.* TDR-EBS-ND-000003 REV 02. Las Vegas, Nevada: Bechtel SAIC Company. ACC: MOL.20011003.0025.

24. Punatar, M.K. 2001. *Summary Report of Commercial Reactor Criticality Data for Crystal River Unit 3.* TDR-UDC-NU-000001 REV 02. Las Vegas, Nevada: Bechtel SAIC Company. ACC: MOL.20010702.0087.

25. AP-3.12Q, Rev. 1, ICN 2. *Design Calculations and Analyses.* Washington, D.C. U.S. Department of Energy, Office of Civilian Radioactive Waste Management. ACC: MOL.20020607.0013.

26. AP-SI.1Q, Rev. 4. *Software Management.* Washington, D.C.: U.S. Department of Energy, Office of Civilian Radioactive Waste Management. ACC: MOL.20030113.0149.

27. BSC (Bechtel SAIC Company) 2003. *21-PWR Waste Package Side and End Impacts.* 000-00C-DSU0-01000-000-00B. Las Vegas, Nevada: Bechtel SAIC Company. ACC: ENG.20030227.0067.

8. ATTACHMENTS

Attachment I (2 pages): Design sketch (*21-PWR Waste Package Configurations for Site Recommendation* [SK-0175 REV 02]. Reference 11 is used in this attachment.)

Attachment II (7 pages): Initial Gap between the Fuel Assemblies and the Inner Shell Bottom Lid

Attachment III (5 pages): Mesh Objectivity

Attachment IV (3 pages): Minimum Output Period for the Results

Attachment V (10 pages): Acceleration Plots Obtained from LS-DYNA

Attachment VI (9 pages): Effect of Ambient Temperature on the Results

Attachment VII (1 page): Natural Frequencies of the Fuel Assemblies (Reference 17 is used in this attachment.)

Attachment VIII (Compact Disc):
ANSYS V5.4 and LS-DYNA electronic files for the end impacts of the 21-PWR waste package. The LS-DYNA input files can be run using either LS-DYNA V950 or LS-DYNA V960.1106. Note that the case "standard mesh, no gap, output period = 0.0001 *s*", is the case 150C\v6. Also, all text editors do not yield the same legibility.

Table 6 lists the name, size, date and time of creation of the files in Attachment VIII.

Table 6. Name, Size, Date and Time of Creation of the Files in Attachment VIII

Directory			
Name	**Size**	**Date**	**Time**
150C\geom			
extract_segments2.inp	1	3/5/2003	12:33 pm
geom1stand6ms3el.inp	64	3/5/2003	12:33 pm
geom1stand6msel.out	788	3/5/2003	12:33 pm
150C\v05			
bcgeom3.inc	4	3/4/2003	03:49 pm
d3hsp	28479	3/4/2003	03:49 pm
d3hsp2	39	3/4/2003	03:49 pm
egeom3.inc	6944	3/4/2003	03:49 pm
ngeom3.inc	6977	3/4/2003	03:48 pm
stand1SR05gloads.k	6	3/4/2003	03:48 pm
stand1SR05gloads2.k	6	3/4/2003	03:48 pm
sym3.inc	41	3/4/2003	03:48 pm
150C\v1			
bcgeom3.inc	4	3/4/2003	03:53 pm
d3hsp	28759	3/4/2003	03:53 pm
egeom3.inc	6944	3/4/2003	03:53 pm
ngeom3.inc	6977	3/4/2003	03:53 pm
stand1SR1gloads.k	6	3/4/2003	03:53 pm
sym3.inc	41	3/4/2003	03:53 pm
150C\v2			
bcgeom3.inc	4	3/4/2003	03:50 pm
d3hsp	28759	3/4/2003	03:50 pm
egeom3.inc	6944	3/4/2003	03:50 pm
ngeom3.inc	6977	3/4/2003	03:50 pm
stand1SR2gloads.k	6	3/4/2003	03:50 pm
sym3.inc	41	3/4/2003	03:50 pm
150C\v4			
bcgeom3.inc	4	3/4/2003	03:51 pm
d3hsp	28759	3/4/2003	03:51 pm
egeom3.inc	6944	3/4/2003	03:50 pm
ngeom3.inc	6977	3/4/2003	03:50 pm
stand1SR4gloads.k	6	3/4/2003	03:50 pm
sym3.inc	41	3/4/2003	03:50 pm

Directory			
Name	**Size**	**Date**	**Time**
150C\v6			
bcgeom3.inc	4	3/4/2003	11:08 am
d3hsp	28759	3/4/2003	11:08 am
egeom3.inc	6944	3/4/2003	11:07 am
ngeom3.inc	6977	3/4/2003	11:07 am
stand1SR6gloads.k	6	3/4/2003	11:07 am
sym3.inc	41	3/4/2003	11:07 am
200C\v1			
bcgeom3.inc	4	3/6/2003	05:51 pm
d3hsp	28759	3/6/2003	05:51 pm
egeom3.inc	6944	3/6/2003	05:51 pm
ngeom3.inc	6977	3/6/2003	05:50 pm
stand1SR1200C.k	6	3/6/2003	05:50 pm
sym3.inc	41	3/6/2003	05:50 pm
200C\v4			
bcgeom3.inc	4	3/6/2003	05:52 pm
d3hsp	28759	3/6/2003	05:52 pm
egeom3.inc	6944	3/6/2003	05:52 pm
ngeom3.inc	6977	3/6/2003	05:52 pm
stand1SR4200C.k	6	3/6/2003	05:52 pm
sym3.inc	41	3/6/2003	05:52 pm
Gap\MaximumGap			
bcgeom3.inc	3	3/4/2003	11:06 am
d3hsp	28486	3/4/2003	11:06 am
d3hsp2	51	3/4/2003	11:06 am
egeom3.inc	6944	3/4/2003	11:06 am
ngeom3.inc	6977	3/4/2003	11:06 am
stand1SR6gapmax.k	6	3/4/2003	11:06 am
sym3.inc	41	3/4/2003	11:06 am
Gap\MediumGap			
bcgeom3.inc	4	3/4/2003	11:04 am
d3hsp	28765	3/4/2003	11:04 am
egeom3.inc	6944	3/4/2003	11:04 am
ngeom3.inc	6977	3/4/2003	11:04 am

Directory			
Name	**Size**	**Date**	**Time**
stand1SR6gloads.k	6	3/4/2003	11:04 am
sym3.inc	41	3/4/2003	11:04 am
Output Period\00005			
bcgeom3.inc	4	2/27/2003	10:11 am
d3hsp	28395	2/27/2003	10:11 am
egeom3.inc	6859	2/27/2003	10:35 am
ngeom3.inc	6857	2/27/2003	10:36 am
stand1SR6gloads.k	6	2/27/2003	10:36 am
sym3.inc	41	2/27/2003	10:36 am
Output Period\0001			
bcgeom3.inc	4	3/5/2003	12:32 pm
d3hsp	28759	3/5/2003	12:32 pm
egeom3.inc	6944	3/5/2003	12:32 pm
ngeom3.inc	6977	3/5/2003	12:31 pm
stand1SR6gloads.k	6	3/5/2003	12:31 pm
sym3.inc	41	3/5/2003	12:31 pm
Refined			
bcgeom3.inc	4	3/4/2003	02:16 pm
d3hsp	32914	3/4/2003	02:16 pm
egeom3.inc	8010	3/4/2003	02:16 pm
extract_segments2.inp	1	3/5/2003	09:46 am
geom1refallFA.inp	64	3/5/2003	09:46 am
geom1refallFA.out	843	3/5/2003	09:46 am
ngeom3.inc	7986	3/4/2003	02:16 pm
refgloadsallFA.k	6	3/4/2003	02:16 pm
sym3.inc	46	3/4/2003	02:16 pm

Note: File size may change with operating system.

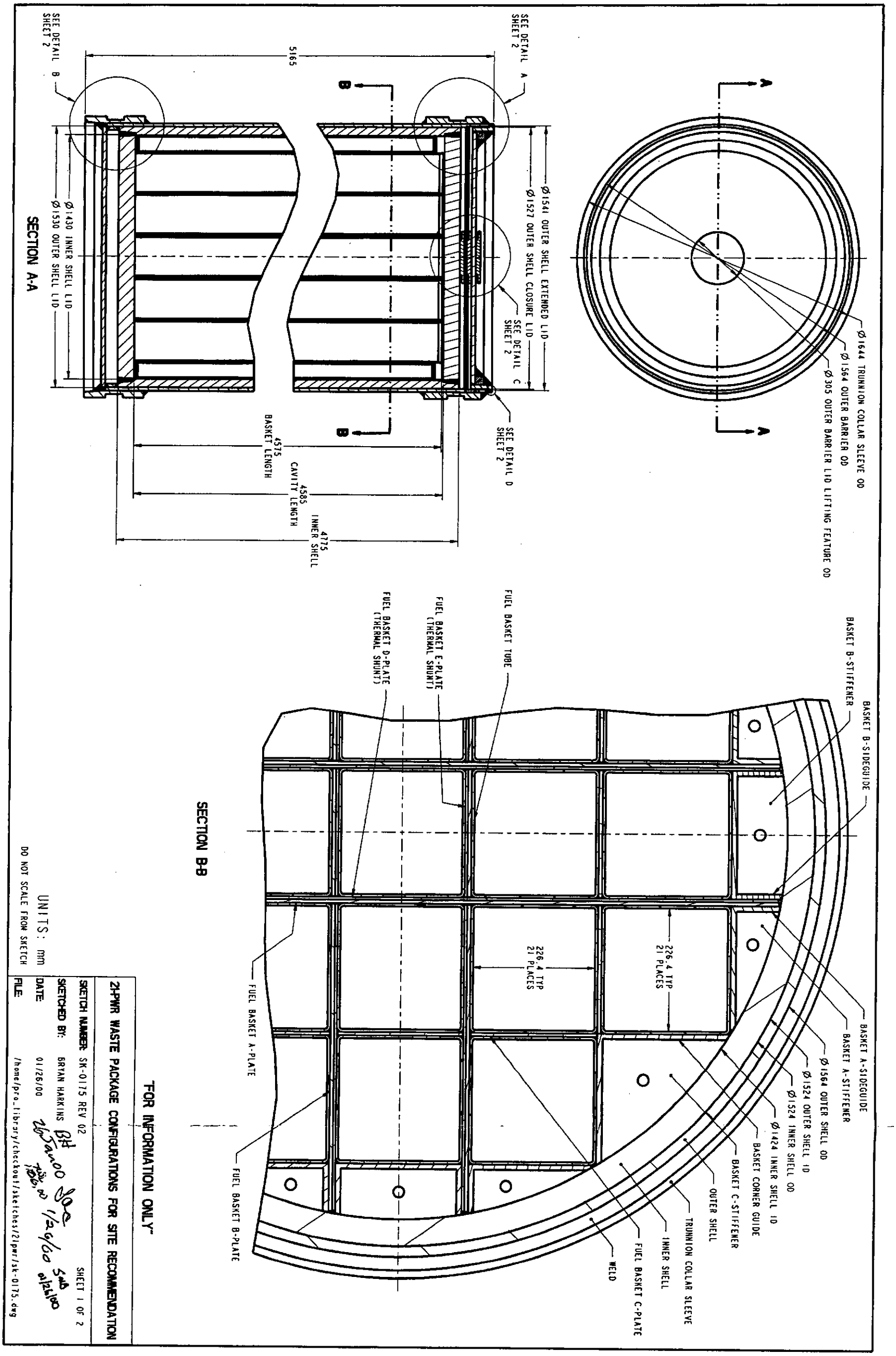

Attachment I: SK-0175 Rev 02 – 21-PWR Waste Package Configurations for Site Recommendation
Originator: VB - March 25,03 Checker: JM 25 March 2003

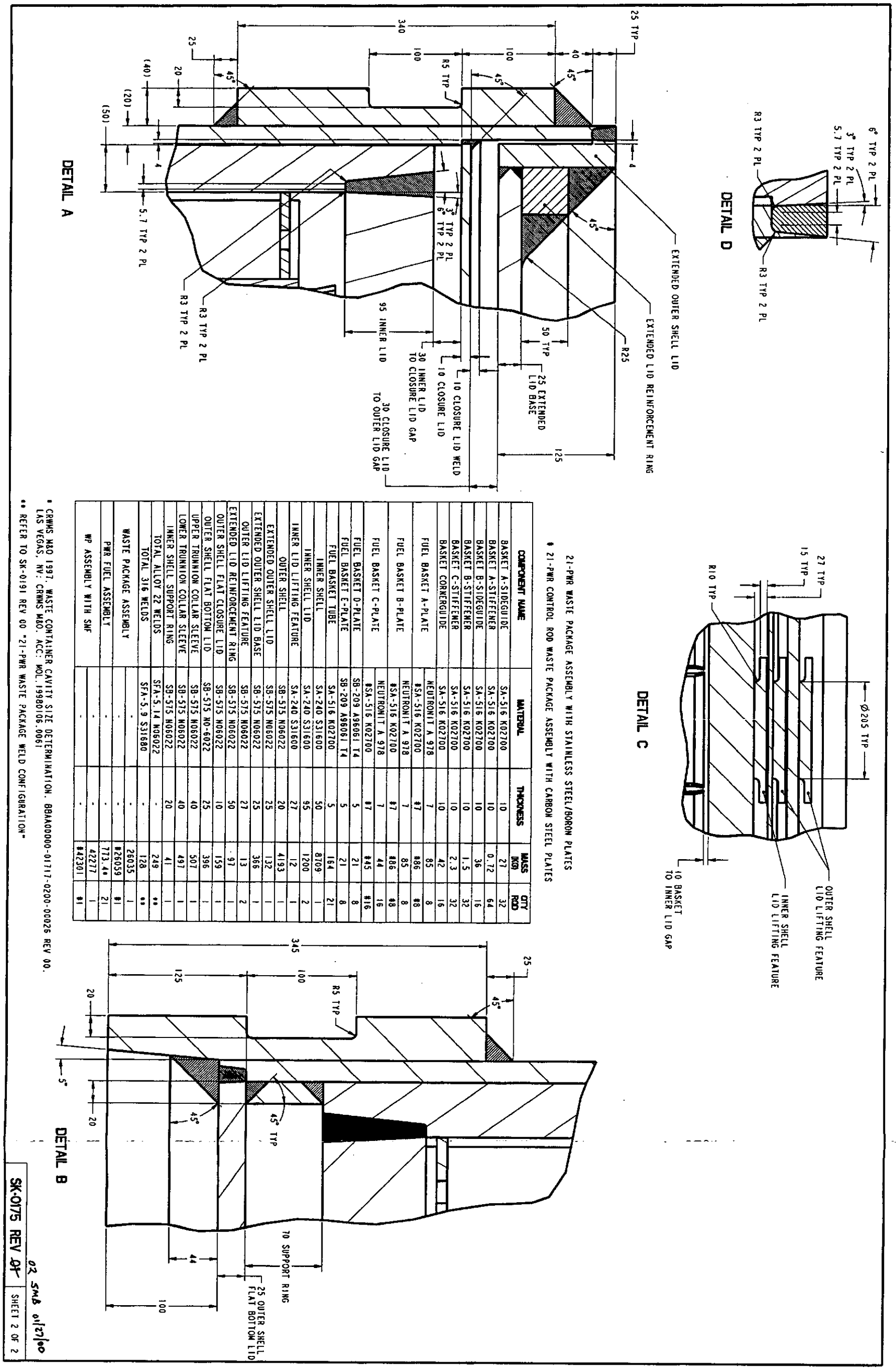

21-PWR WASTE PACKAGE ASSEMBLY WITH STAINLESS STEEL/BORON PLATES

21-PWR CONTROL ROD WASTE PACKAGE ASSEMBLY WITH CARBON STEEL PLATES

COMPONENT NAME		MATERIAL	THICKNESS	MASS (KG)	QTY ROD
BASKET A-SIDEGUIDE		SA-516 K02700	10	27	32
BASKET A-STIFFENER		SA-516 K02700	10	0.72	64
BASKET B-SIDEGUIDE		SA-516 K02700	10	36	16
BASKET B-STIFFENER		SA-516 K02700	10	1.5	32
BASKET C-STIFFENER		SA-516 K02700	10	2.3	32
BASKET CORNERGUIDE		SA-516 K02700	10	42	16
FUEL BASKET A-PLATE		NEUTRONIT A 978	7	85	8
FUEL BASKET B-PLATE		#SA-516 K02700	#7	#86	#8
		NEUTRONIT A 978	7	85	8
		#SA-516 K02700	#7	#86	#8
		NEUTRONIT A 978	7	44	16
FUEL BASKET C-PLATE		#SA-516 K02700	#7	#45	#16
FUEL BASKET D-PLATE		SB-209 A96061 T4	5	21	8
FUEL BASKET E-PLATE		SB-209 A96061 T4	5	21	8
FUEL BASKET TUBE		SA-516 K02700	5	164	21
INNER SHELL		SA-240 S31600	50	8709	1
INNER SHELL LID		SA-240 S31600	95	1200	2
INNER LID LIFTING FEATURE		SA-240 S31600	27	12	1
OUTER SHELL		SB-575 N06022	20	4193	1
EXTENDED OUTER SHELL LID		SB-575 N06022	25	132	1
EXTENDED OUTER SHELL LID BASE		SB-575 N06022	25	366	1
OUTER LID LIFTING FEATURE		SB-575 N06022	27	13	2
EXTENDED LID REINFORCEMENT RING		SB-575 N06022	50	97	1
OUTER SHELL FLAT CLOSURE LID		SB-575 N06022	10	159	1
OUTER SHELL FLAT BOTTOM LID		SB-575 N0-6022	25	396	1
UPPER TRUNNION COLLAR SLEEVE		SB-575 N06022	40	507	1
LOWER TRUNNION COLLAR SLEEVE		SB-575 N06022	40	497	1
INNER SHELL SUPPORT RING		SB-575 N06022	20	41	1
TOTAL ALLOY 22 WELDS		SFA-5.14 N06022	-	249	**
TOTAL 316 WELDS		SFA-5.9 S31680	-	128	**
WASTE PACKAGE ASSEMBLY		-	-	26035	1
PWR FUEL ASSEMBLY		-	-	#26059	#1
WP ASSEMBLY WITH SNF		-	-	773.4*	21
		-	-	42277	1
		-	-	#42301	#1

* CRWMS M&O 1997. WASTE CONTAINER CAVITY SIZE DETERMINATION. BBAA00000-01717-0200-00026 REV 00. LAS VEGAS, NV: CRWMS M&O. ACC: MOL.19980106.0061

** REFER TO SK-0191 REV 00 "21-PWR WASTE PACKAGE WELD CONFIGURATION"

SK-0175 REV 02 SHEET 2 OF 2

02 SMB 01/27/00

ATTACHMENT II
INITIAL GAP BETWEEN THE FUEL ASSEMBLIES AND THE INNER SHELL BOTTOM LID

The object of this attachment is to study the effect of the initial gap (distance) between the fuel assemblies and the IS bottom lid, in order to ensure that the configuration used yields the maximum acceleration.

Three gap values are studied: In the first case, the gap between the fuel assemblies and the IS bottom lid is very small (0.1 *mm*), and this initial configuration will be called "no gap" throughout this section. In the second case, the fuel assemblies are axially centered in the IS cavity (medium gap). In the third case, the gap between the fuel assemblies and the IS bottom lid is maximum.

An initial velocity of 6 *m/s* is used for this study. Tables II-1 to II-3 give the maximum accelerations obtained for these three different gaps, in three fuel assemblies. The position of the fuel assemblies is illustrated in Figure II- 1. Butterworth filter is used with three different cutoff frequencies. The cutoff frequencies are chosen based on discussion presented in Attachment VII.

Table II- 1. Maximum Acceleration (*g*) for three Fuel Assemblies, with no Gap at the Beginning of the Simulation

	Cutoff Frequency (*Hz*)		
Fuel Assembly Number (See Figure II- 1)	**450 (See Figure II- 2)**	**600 (See Figure II- 3)**	**1000 (See Figure II- 4)**
1 (node # 287)	506	567	701
2 (node # 1114)	152	169	213
3 (node # 5489)	180	205	265

Table II- 2. Maximum Acceleration (*g*) for three Fuel Assemblies, with a Medium Gap at the Beginning of the Simulation

	Cutoff Frequency (*Hz*)		
Fuel Assembly Number (See Figure II- 1)	**450 (See Figure II- 5)**	**600 (See Figure II- 6)**	**1000 (See Figure II- 7)**
1 (node # 287)	465	554	646
2 (node # 1114)	214	284	493
3 (node # 5489)	293	344	438

Table II- 3. Maximum Acceleration (*g*) for three Fuel Assemblies, with a Maximum Gap at the Beginning of the Simulation

	Cutoff Frequency (*Hz*)		
Fuel Assembly Number (See Figure II- 1)	**450 (See Figure II- 8)**	**600 (See Figure II- 9)**	**1000 (See Figure II- 10)**
1 (node # 287)	203	235	374
2 (node # 1114)	157	191	264
3 (node # 5489)	282	322	418

These results show that for all three fuel assemblies, the configuration where there is no initial gap between the fuel assemblies and the IS bottom lid yields the most conservative maximum acceleration. This geometrical configuration will be used for the remainder of the study.

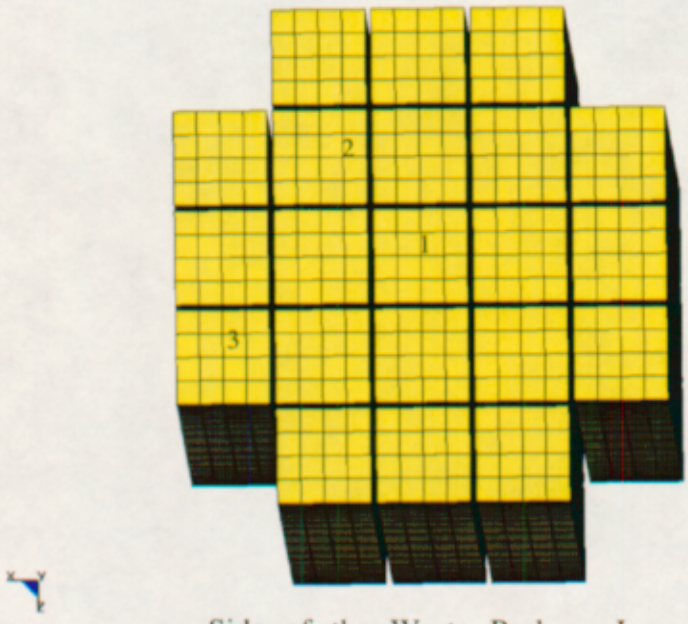

Side of the Waste Package Impacting the Unyielding Surface

Figure II- 1. Position of the Fuel Assemblies used in the Gap Study

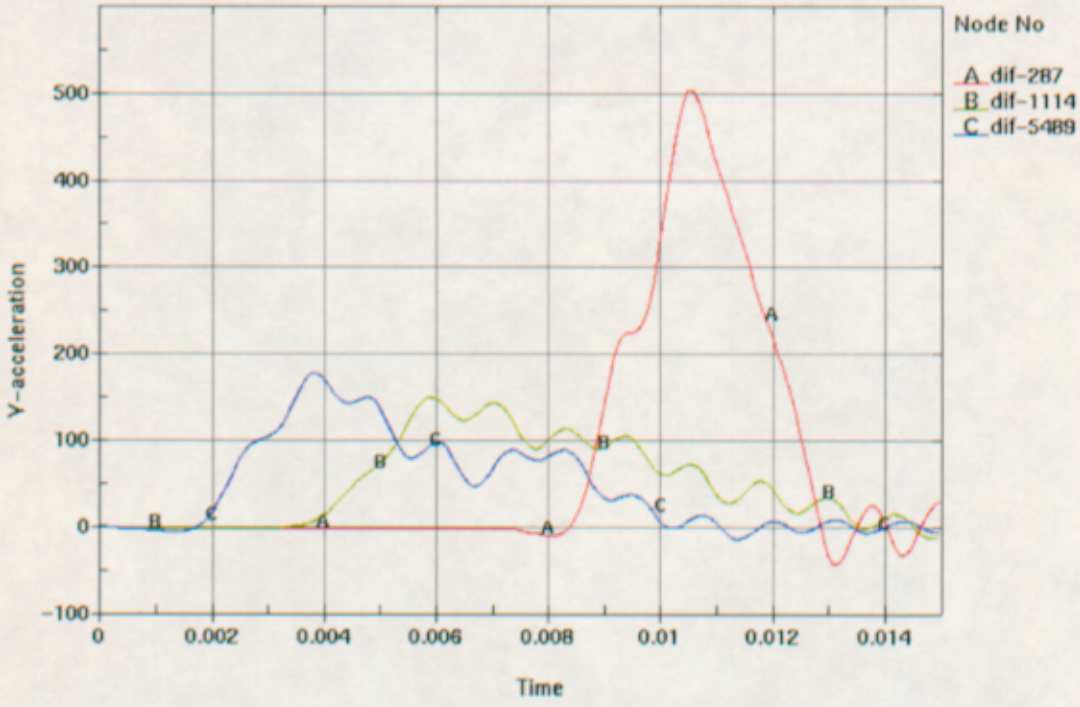

Figure II- 2. Acceleration (*g*) for three Fuel Assemblies, no Gap, Cutoff Frequency 450 *Hz*

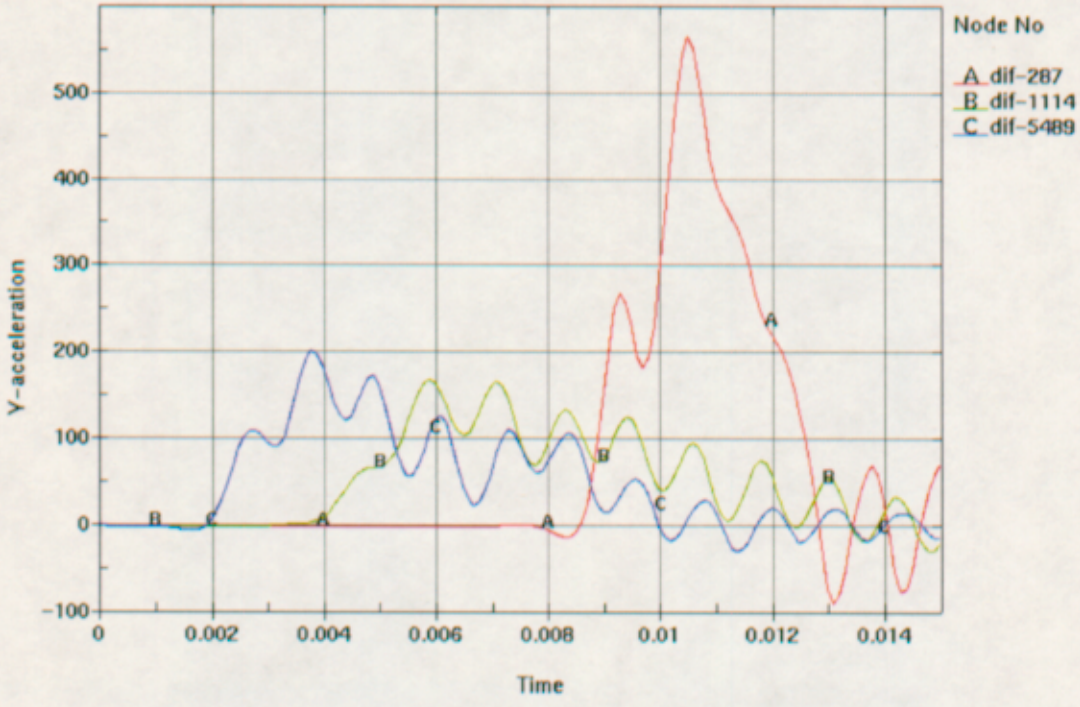

Figure II- 3. Acceleration (*g*) for three Fuel Assemblies, no Gap, Cutoff Frequency 600 *Hz*

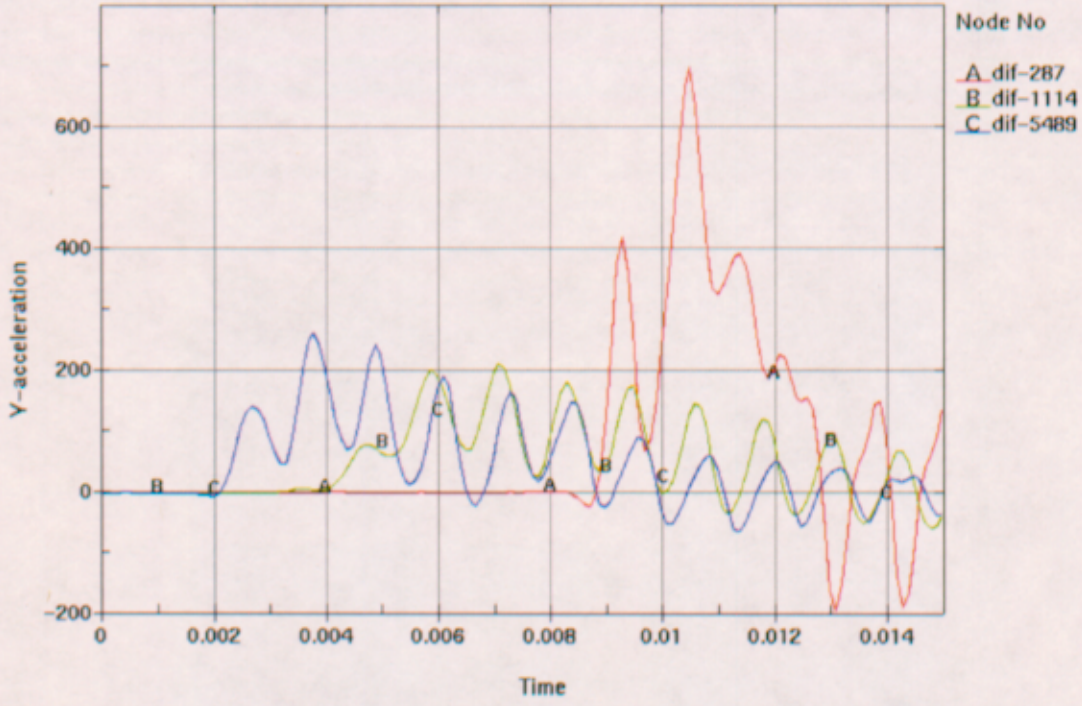

Figure II- 4. Acceleration (*g*) for three Fuel Assemblies, no Gap, Cutoff Frequency 1000 *Hz*

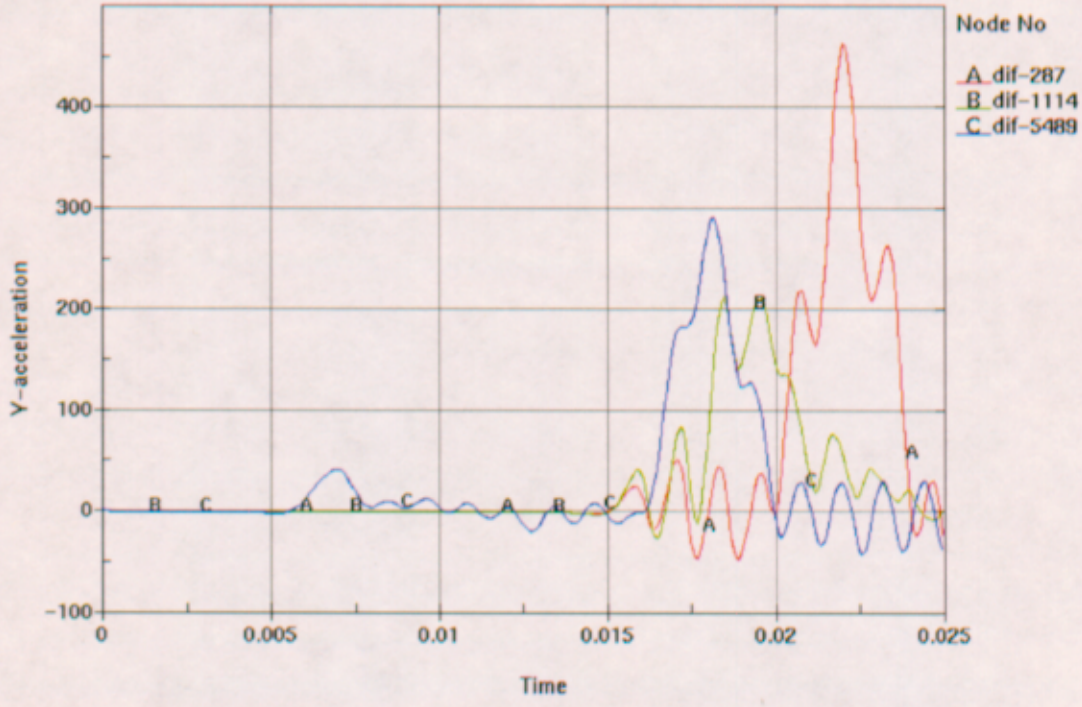

Figure II- 5. Acceleration (*g*) for three Fuel Assemblies, Medium Gap, Cutoff Frequency 450 *Hz*

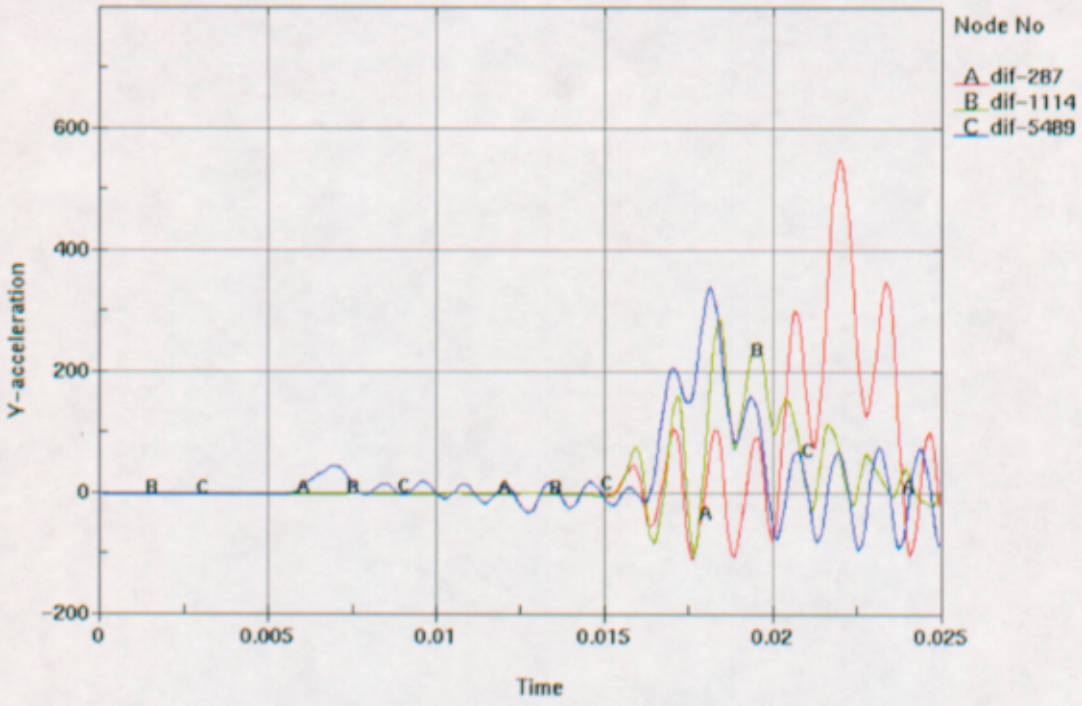

Figure II- 6. Acceleration (*g*) for three Fuel Assemblies, Medium Gap, Cutoff Frequency 600 *Hz*

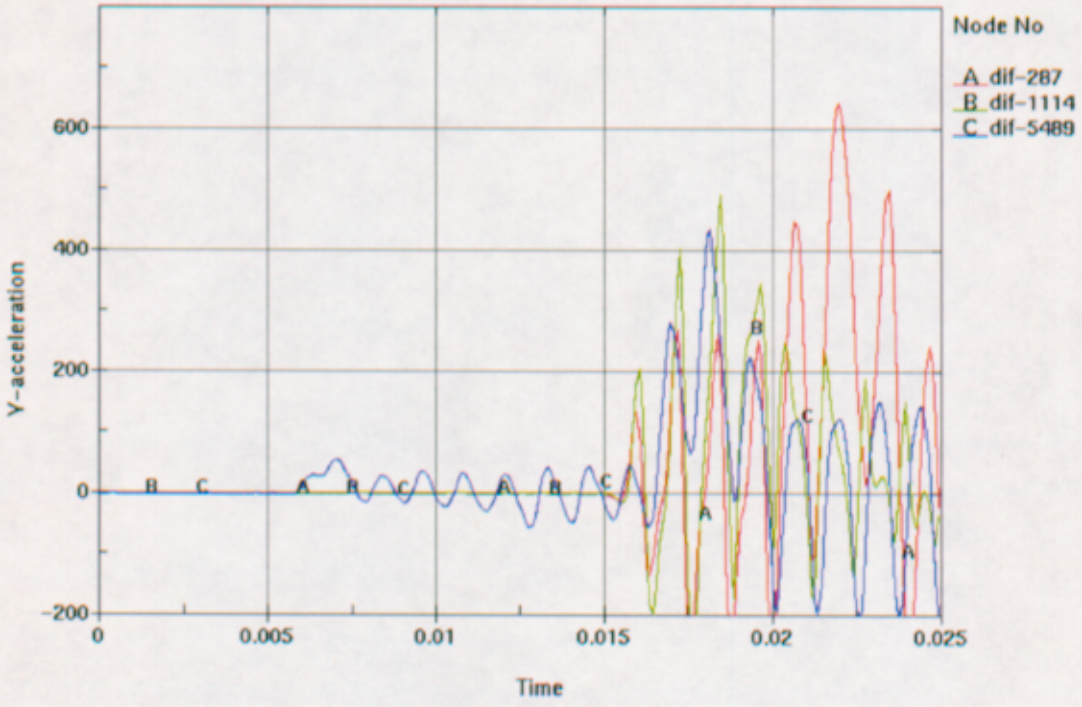

Figure II- 7. Acceleration (*g*) for three Fuel Assemblies, Medium Gap, Cutoff Frequency 1000 *Hz*

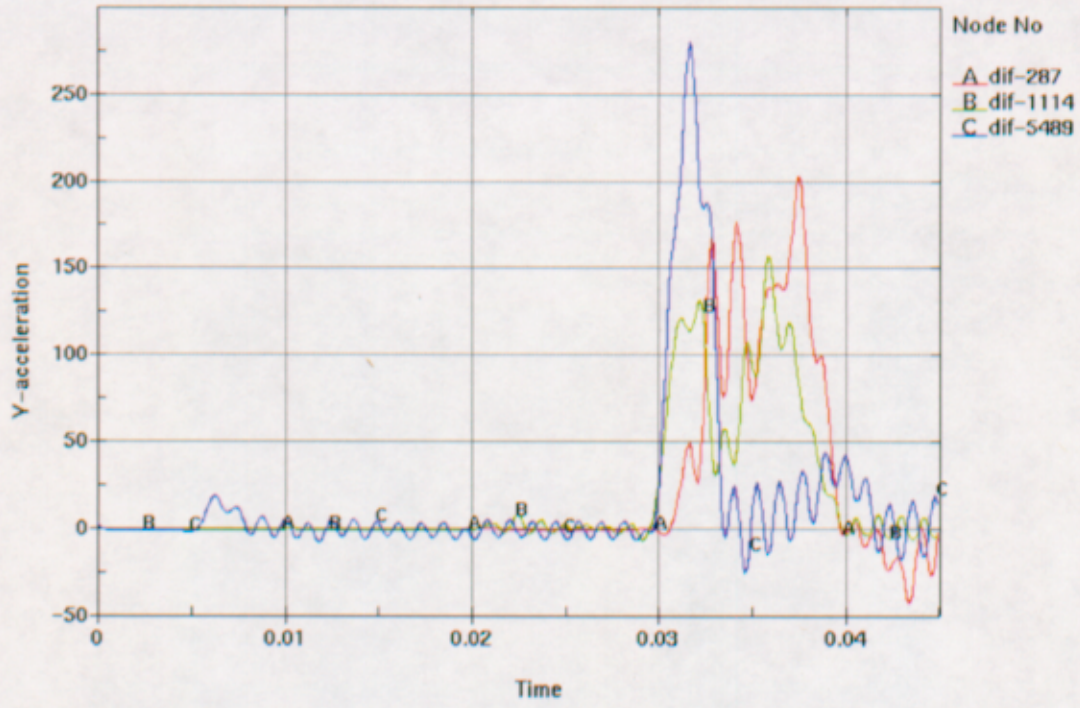

Figure II- 8. Acceleration (*g*) for three Fuel Assemblies, Maximum Gap, Cutoff Frequency 450 *Hz*

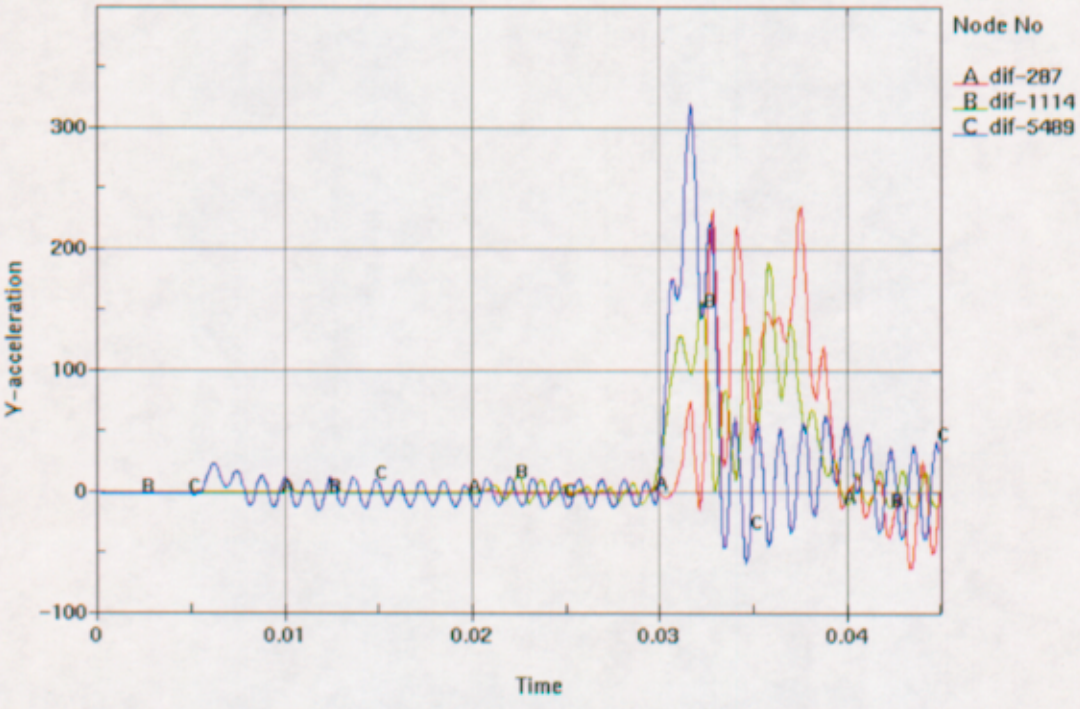

Figure II- 9. Acceleration (*g*) for three Fuel Assemblies, Maximum Gap, Cutoff Frequency 600 *Hz*

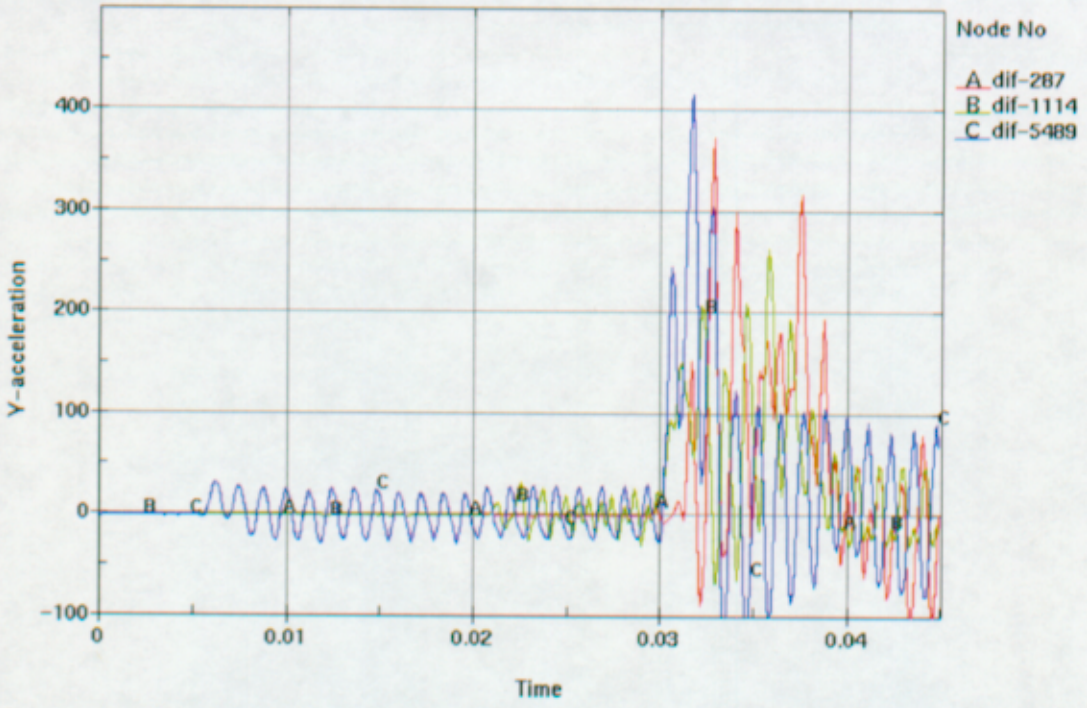

Figure II- 10. Acceleration *(g)* for three Fuel Assemblies, Maximum Gap, Cutoff Frequency 1000 *Hz*

ATTACHMENT III
MESH OBJECTIVITY

The object of this attachment is to verify that the results are not mesh-sensitive (i.e., that a small perturbation of the mesh does not change the results). A mesh is generated according to standard engineering practice (see Ref. 20, Section 6.2.3) (this mesh is called "standard mesh" in this document). The mesh is then refined in the contact region (fuel assemblies and IS bottom lid) (this mesh is called "refined mesh" in this document). The difference in maximum acceleration obtained in three fuel assemblies between the two meshes is compared to the variation in volume of an element representative of the mesh according to the method described in Reference 20, Section 6.2.3. The three fuel assemblies used for this study are these defined in Figure II-1. The nodes corresponding to the fuel assemblies number 1, 2 and 3 in the refined mesh are nodes number 545, 2404 and 10572, respectively. An initial velocity of 6 *m/s* is used.

Table III- 1 and III- 2 give the maximum accelerations obtained for two different meshes. Butterworth filter is used with three different cutoff frequencies.

Table III- 1. Maximum Acceleration *(g)* for three Fuel Assemblies, Standard Mesh

	Cutoff Frequency (*Hz*)		
Fuel Assembly Number (See Figure II- I)	**450 (See Figure II- 2)**	**600 (See Figure II- 3)**	**1000 (See Figure II- 4)**
1 (node # 287)	506	567	701
2 (node # 1114)	152	169	213
3 (node # 5489)	180	205	265

Table III- 2. Maximum Acceleration *(g)* for three Fuel Assemblies, Refined Mesh

	Cutoff Frequency (*Hz*)		
Fuel Assembly Number (See Figure II- I)	**450 (See Figure III- 1)**	**600 (See Figure III- 2)**	**1000 (See Figure III- 3)**
1 (node # 545)	492	549	674
2 (node # 2404)	145	164	214
3 (node # 10572)	177	202	260

Table III- 3 shows the relative difference in results between the two different meshes described above. Table III- 4 shows the relative difference in volume for representative elements for the two meshes.

Table III- 3. Comparison between the Results Obtained with the Standard Mesh and the Refined Mesh (%)

	Relative Difference in Maximum Acceleration (%), with a Cutoff Frequency of (*Hz*)		
Fuel Assembly Number (See Figure II- I)	**450**	600	1000
1	-2.8	-3.3	-4.0
2	-4.8	-3.0	0.5
3	-1.7	-1.5	-1.9

Table III- 4. Comparison of the Volume of a Representative Element of the Standard Mesh and of the Refined Mesh (%)

	Standard Mesh	**Refined Mesh**	**Relative Difference between Standard and Refined (%)**
Volume of a Representative Element of the IS (m^3) (Element Number)	$1.7606 \cdot 10^{-5}$ (# 43590)	$9.1897 \cdot 10^{-6}$ (# 52300)	-92
Volume of a Representative Element of the Fuel Assemblies (m^3) (Element Number)	$2.3863 \cdot 10^{-4}$ (# 3193)	$8.8831 \cdot 10^{-5}$ (# 49)	-170

These results show that in all cases, the results from the standard mesh are higher that the results from the refined mesh, and that the criterion defined in Reference 20, Section 6.2.3 is met. Therefore, the standard mesh is deemed acceptable, and is used for the remainder of the simulations. A picture of the standard mesh is presented in Figure III- 4.

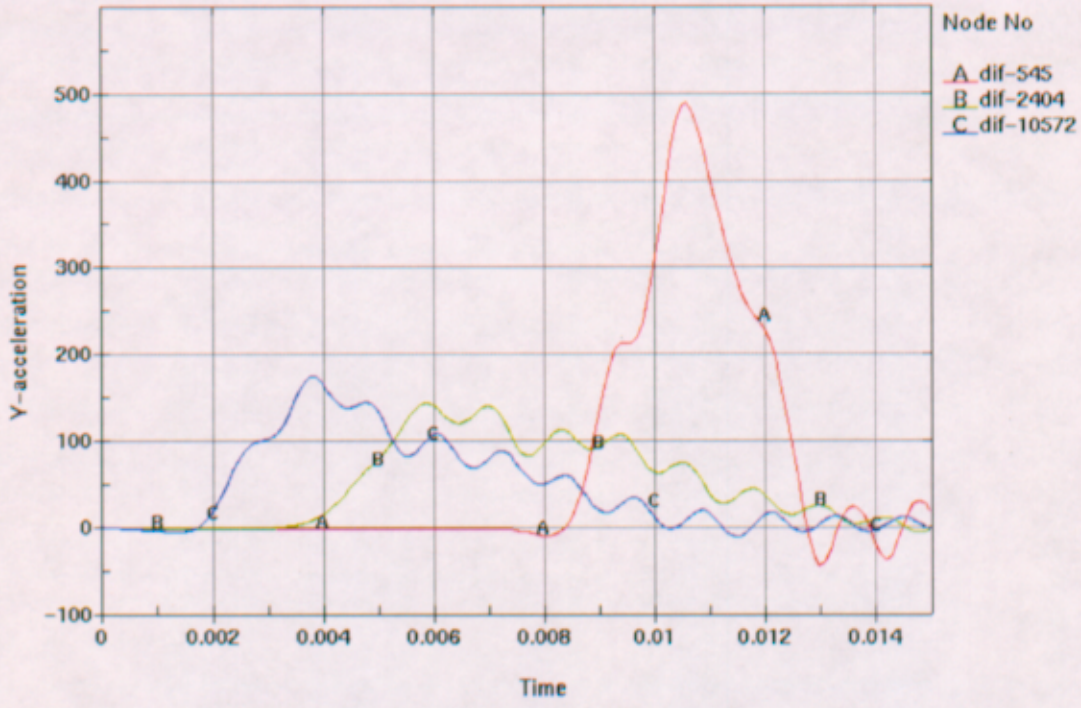

Figure III- 1. Accelerations (*g*) for three Fuel Assemblies, Refined Mesh, Cutoff Frequency 450 *Hz*

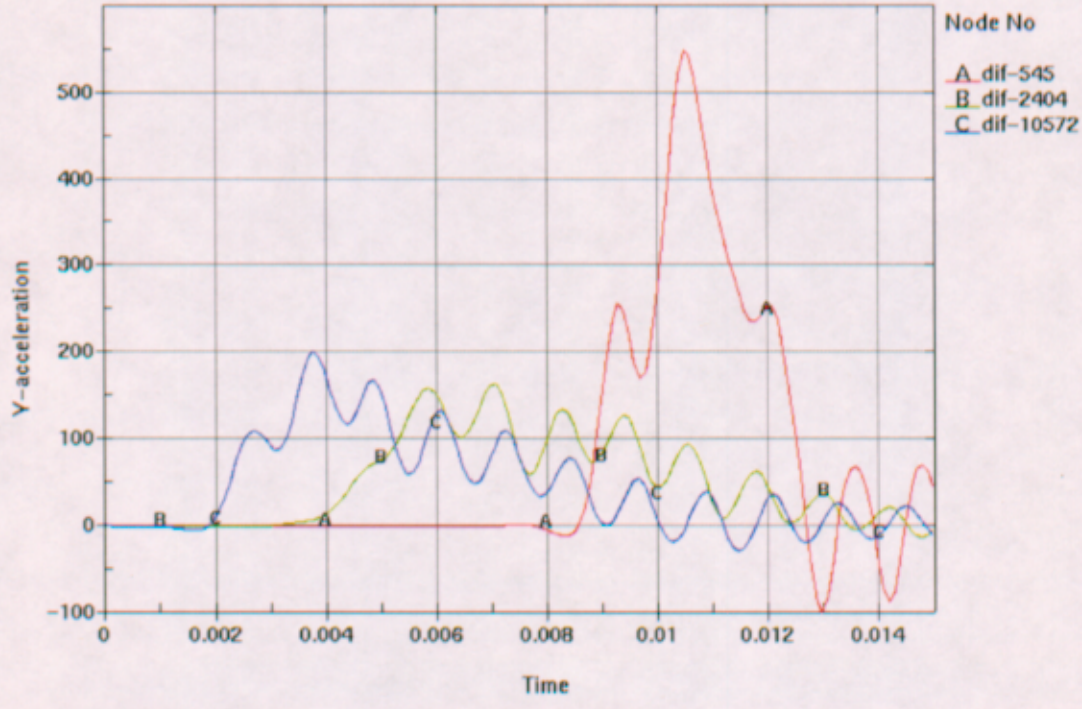

Figure III- 2. Accelerations (*g*) for three Fuel Assemblies, Refined Mesh, Cutoff Frequency 600 *Hz*

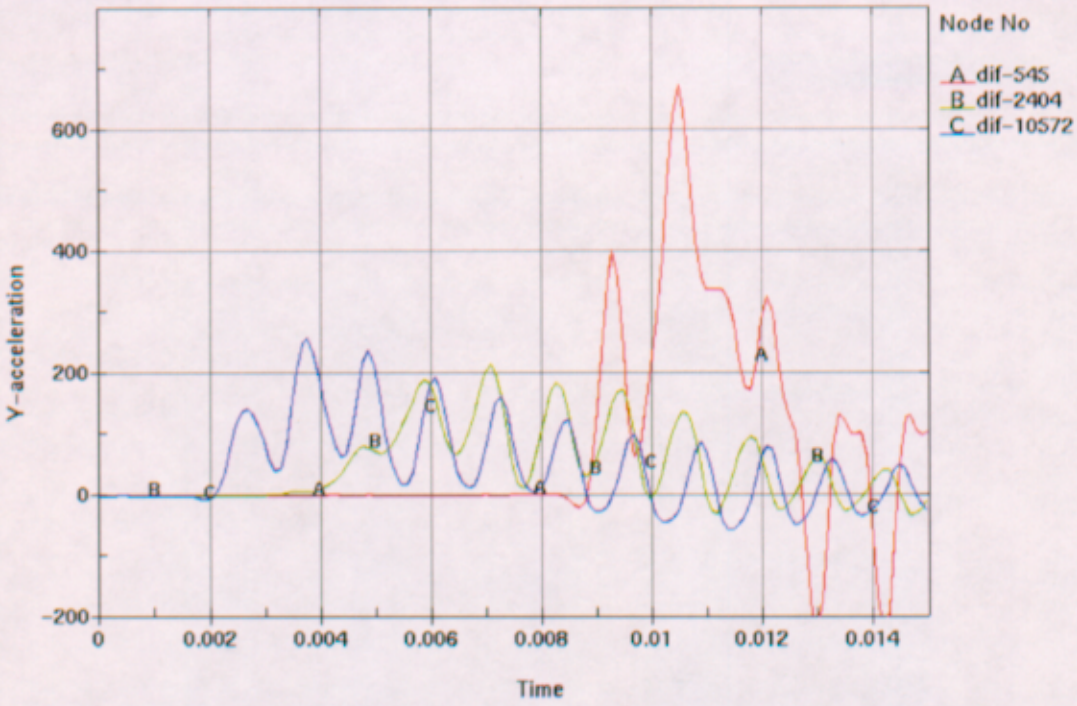

Figure III- 3. Accelerations (*g*) for three Fuel Assemblies, Refined Mesh, Cutoff Frequency 1000 *Hz*

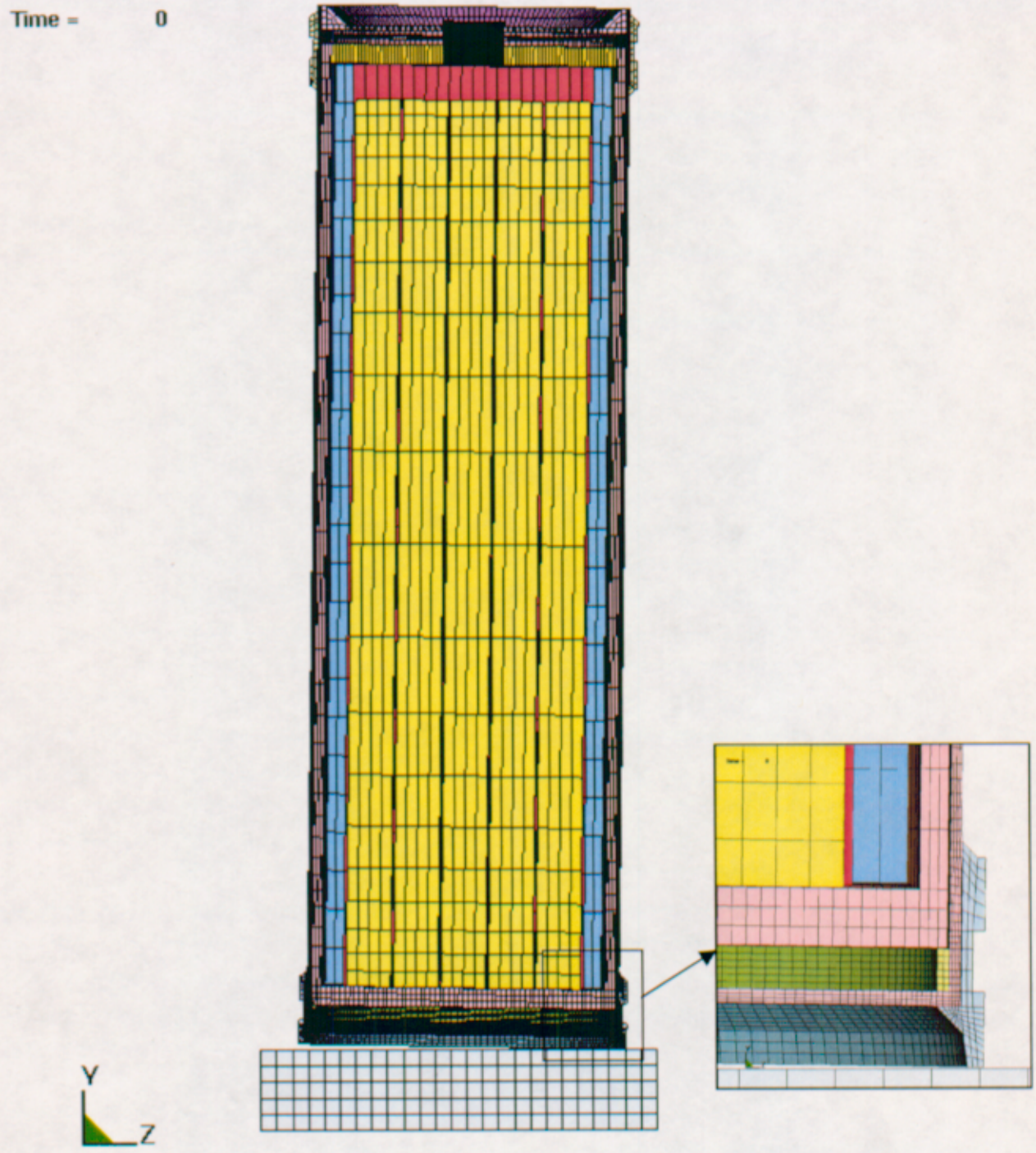

Figure III- 4. Standard Mesh

ATTACHMENT IV
MINIMUM OUTPUT PERIOD FOR THE RESULTS

During the simulations, the results are recorded at a frequency defined by the user. In order to capture the maximum value of accelerations, the frequency at which the results are recorded must be high enough. The object of this attachment is to determine the minimum output period necessary to ensure that the maximum accelerations will be captured, without creating an unnecessary large number of result files.

The initial output period is 0.005 *s*. This output period is diminished until the percentage difference in maximum acceleration is an order of magnitude smaller than the percentage difference in output period. The initial velocity of the waste package used for this study is 6 *m/s*.

Tables IV- 1 and IV- 2 present the maximum accelerations obtained in three fuel assemblies for the two cases that meet the criterion defined above. Butterworth filtering is used with three different cutoff frequencies. The position of the fuel assemblies is shown in Figure II- 1.

Table IV- 1. Maximum Acceleration (*g*) for three Fuel Assemblies, Output Period of 0.0001 *s*

	Cutoff Frequency (*Hz*)		
Fuel Assembly Number (See Figure II- 1)	**450 (See Figure II- 2)**	**600 (See Figure II- 3)**	**1000 (See Figure II-4)**
1 (node # 287)	506	567	701
2 (node # 1114)	152	169	213
3 (node # 5489)	180	205	265

Table IV- 2. Maximum Acceleration (*g*) for three Fuel Assemblies, Output Period of 0.00005 *s*

	Cutoff Frequency (*Hz*)		
Fuel Assembly Number (See Figure II- 1)	**450 (See Figure IV- 1)**	**600 (See Figure IV- 2)**	**1000 (See Figure IV- 3)**
1 (node # 287)	510	567	702
2 (node # 1114)	152	164	212
3 (node # 5489)	181	206	266

Table IV- 3 presents the relative difference of maximum acceleration between the two cases.

Table IV- 3. Comparison between the two Cases with Different Output Periods

	Relative Difference in Acceleration (%), with Cutoff Frequency of		
Fuel Assembly Number (See Figure II- 1)	450 *Hz*	600 *Hz*	1000 *Hz*
1 (node # 287)	0.8	0	0.1
2 (node # 1114)	0	-3.0	-0.5
3 (node # 5489)	0.6	-0.5	0.4

The relative difference in output period between the two cases is 100%. This shows that the results are stable for an output period of 0.0001 *s*. This output period is used for the remainder of the simulations.

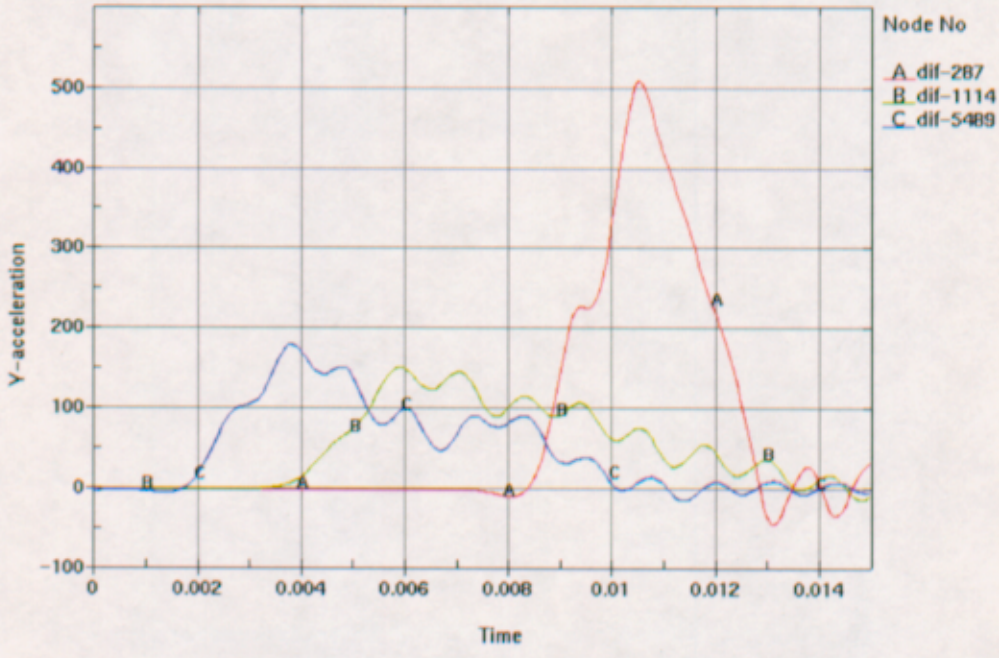

Figure IV- 1. Accelerations (*g*) for three Fuel Assemblies, Output Period 0.00005 *s*, Cutoff Frequency 450 *Hz*

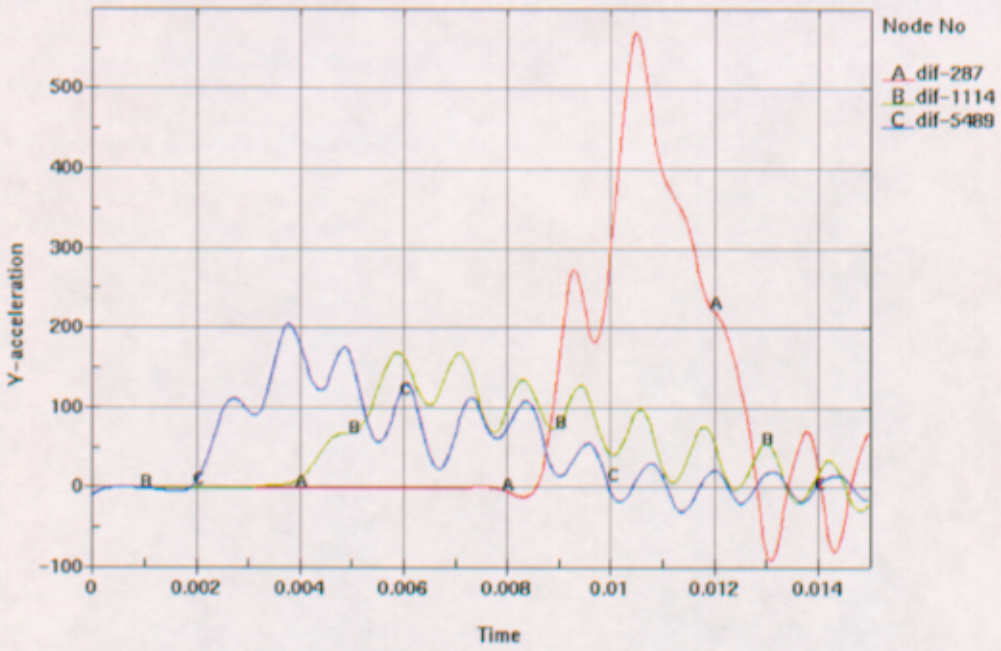

Figure IV- 2. Accelerations (*g*) for three Fuel Assemblies, Output Period 0.00005 *s*, Cutoff Frequency 600 *Hz*

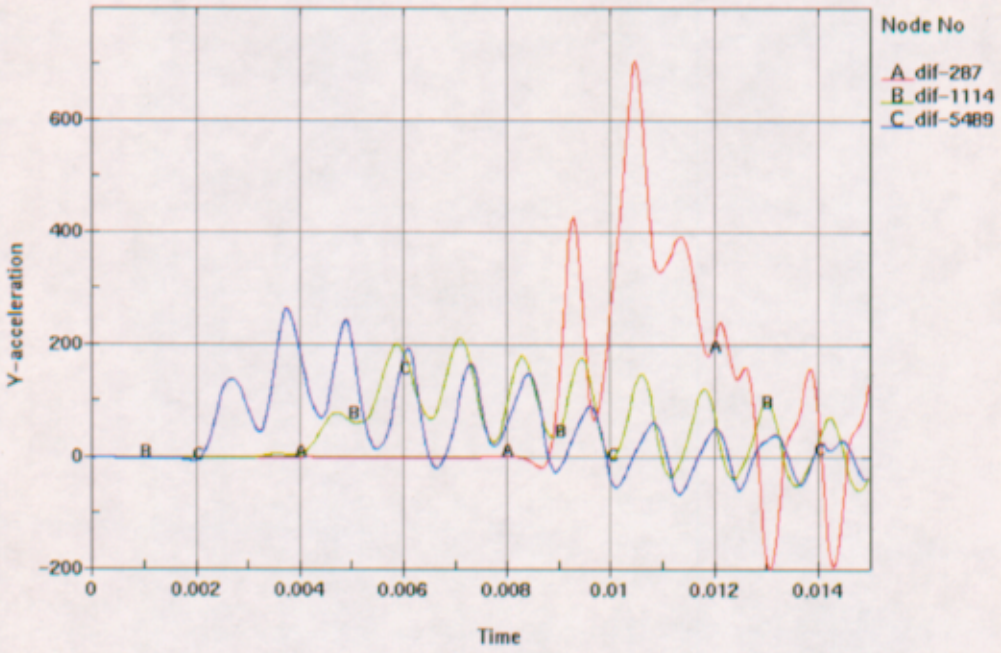

Figure IV- 3. Accelerations (*g*) for three Fuel Assemblies, Output Period 0.00005 *s*, Cutoff Frequency 1000 *Hz*

ATTACHMENT V
ACCELERATION PLOTS OBTAINED FROM LS-DYNA

The object of this attachment is to illustrate the acceleration time histories corresponding to the results presented in Tables 4 and 5 of this document. Butterworth filter is used with three different cutoff frequencies to remove high-frequency response. For two cases (initial velocity = 1 *m/s*, cutoff frequencies 450 *Hz* and 600 *Hz*), the calculation of the average peak acceleration is given in details.

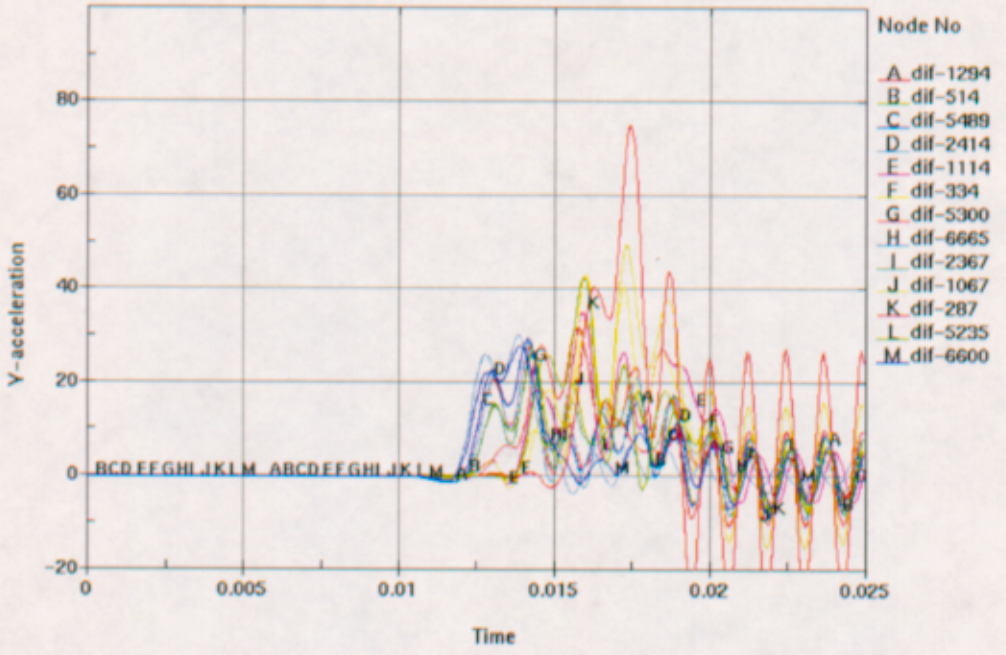

Figure V- 1. Accelerations plot (*g*), Initial Velocity = 0.5 *m/s*, T = 150 *°C*, Cutoff Frequency 450 *Hz*

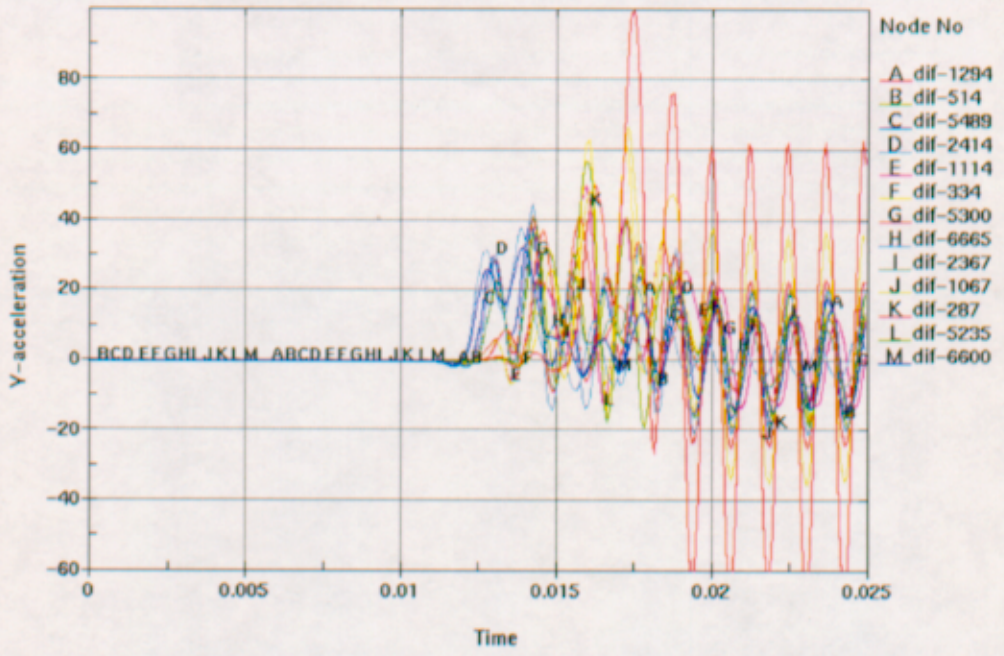

Figure V- 2. Accelerations plot (*g*), Initial Velocity = 0.5 *m/s*, T = 150 *°C*, Cutoff Frequency 600 *Hz*

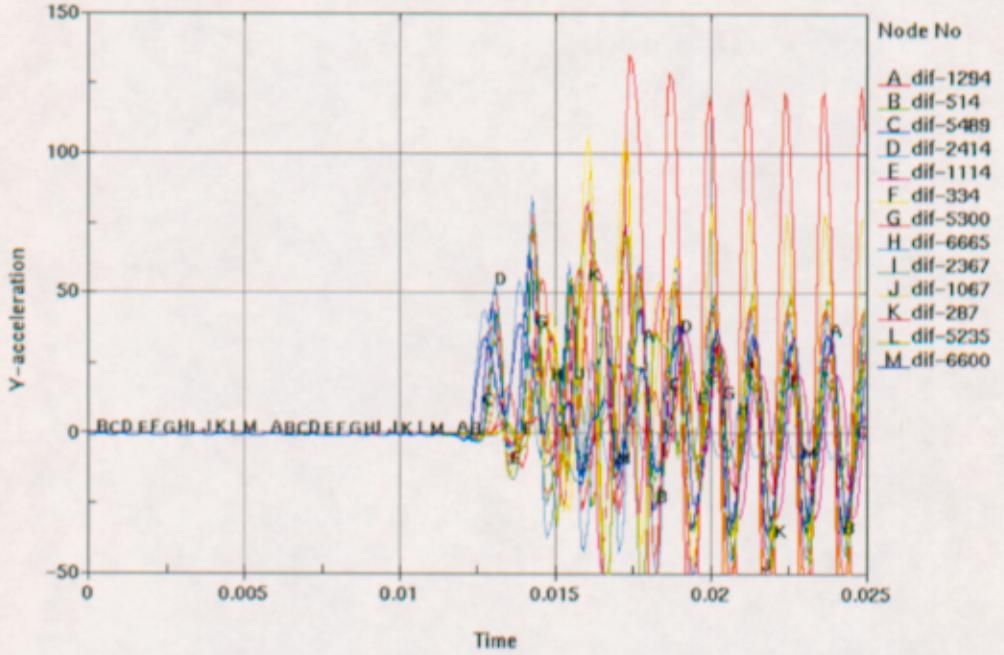

Figure V- 3. Accelerations plot (*g*), Initial Velocity = 0.5 *m/s*, T = 150 *°C*, Cutoff Frequency 1000 *Hz*

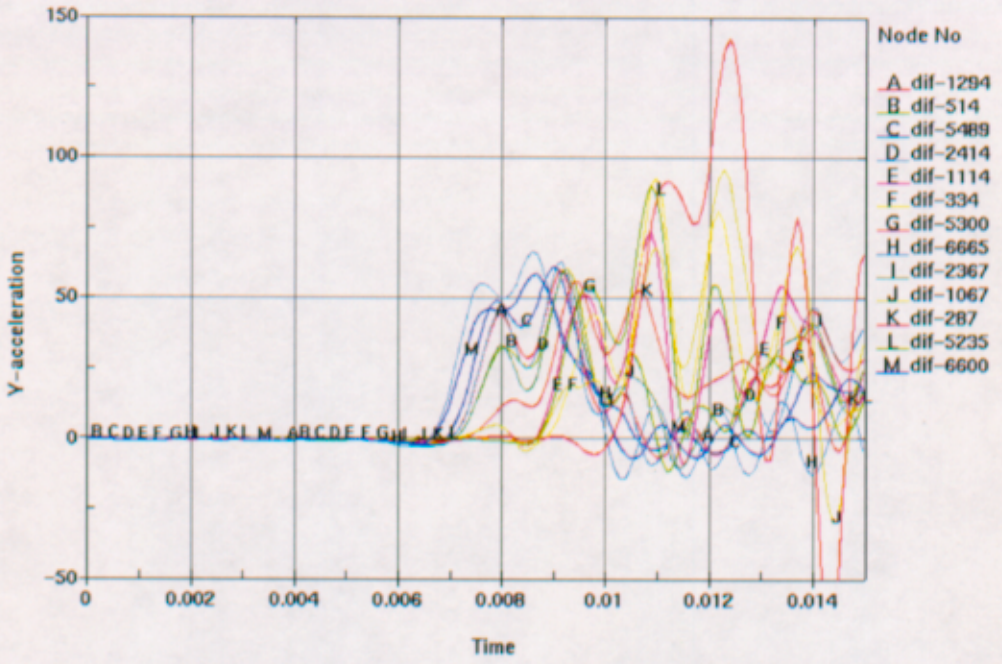

Figure V- 4. Accelerations plot (*g*), Initial Velocity = 1 *m/s*, T = 150 *°C*, Cutoff Frequency 450 *Hz*

Table V- 1 shows the peak acceleration for each fuel assembly in the case where the initial velocity is 1 *m/s* and the cutoff frequency 450 *Hz*, in order to illustrate the way the average peak acceleration is calculated. Figure V- 5 shows the correspondence between the node number and the location of the fuel assembly in the FER.

Table V- 1. Maximum Acceleration (*g*) on each Fuel Assembly, Initial Velocity = 1 *m/s*, T = 150 *°C*, Cutoff Frequency 450 *Hz*

Node #	Peak Acceleration	Node #	Peak Acceleration	Node #	Peak Acceleration
1294	60	2414	63	2367	60
514	61	1114	74	1067	96
5489	61	334	93	287	144
		5300	56	5235	91
		6665	67	6600	59

As shown in Figure V- 5, the FER is half-symmetric. Hence, the values of acceleration in the fuel assemblies that are not on the plane of symmetry should be taken into account twice in the calculation of the average peak acceleration, in order to compensate for the fuel assemblies that are

not represented in the FER. In Tables V- 1 and V- 2, the peak accelerations taken into account twice are in bold.

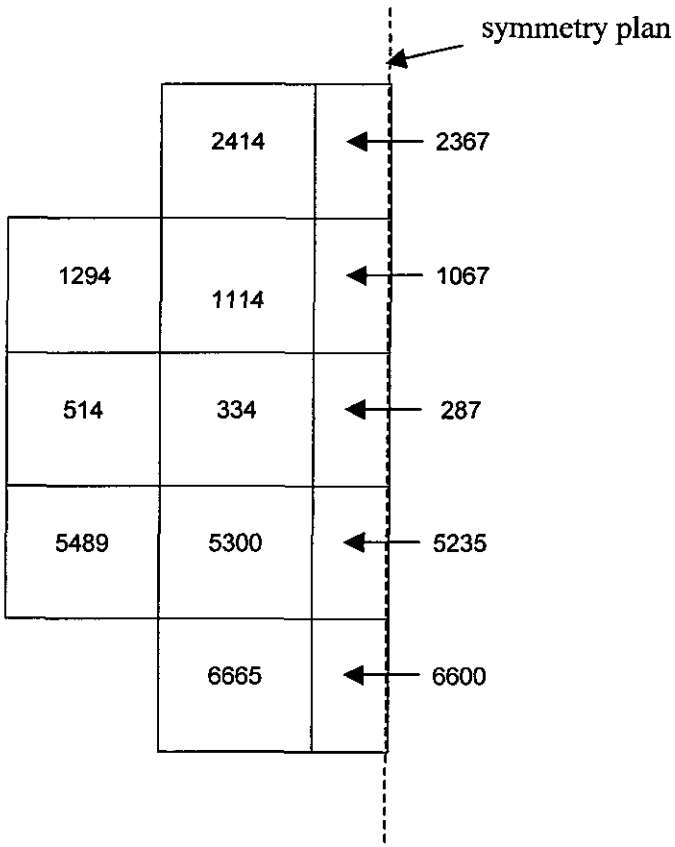

Figure V- 5. Correspondence between Node Number and Fuel Assembly Position in the FER.

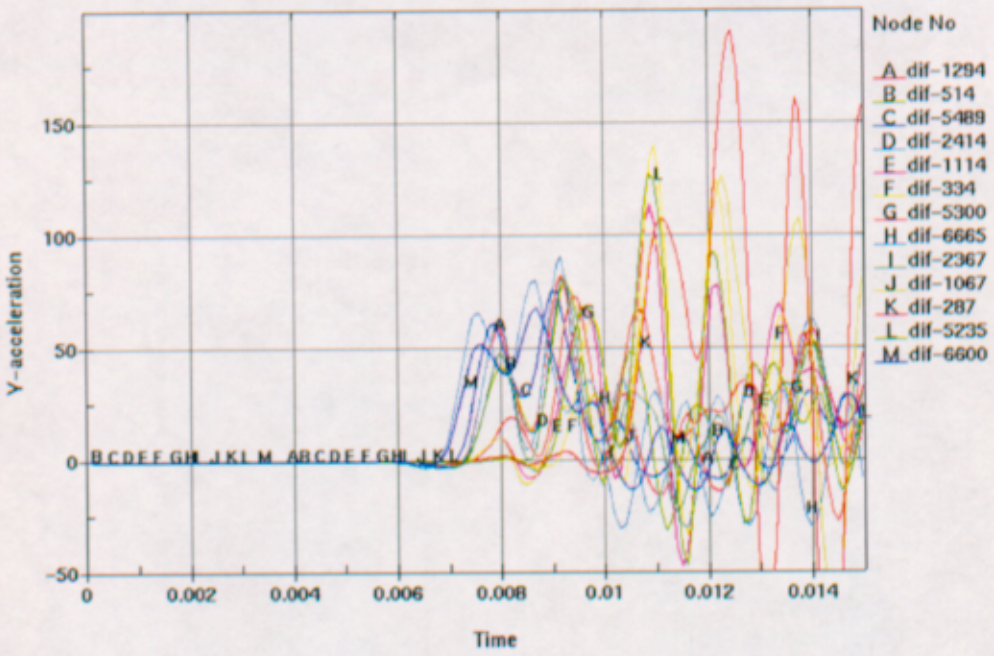

Figure V- 6. Accelerations plot (*g*), Initial Velocity = 1 *m/s*, T = 150 °C, Cutoff Frequency 600 *Hz*

Table V- 2 shows the peak acceleration for each fuel assembly in the case where the initial velocity is 1 *m/s* and the cutoff frequency 600 *Hz*, for illustration purposes.

Table V- 2. Peak Acceleration (*g*) on each Fuel Assembly, Initial Velocity = 1 *m/s*, T = 150 °C, Cutoff Frequency 600 *Hz*

Node #	Peak Acceleration	Node #	Peak Acceleration	Node #	Peak Acceleration
1294	83	2414	92	2367	82
514	80	1114	114	1067	126
5489	75	334	140	287	192
		5300	73	5235	128
		6665	81	6600	68

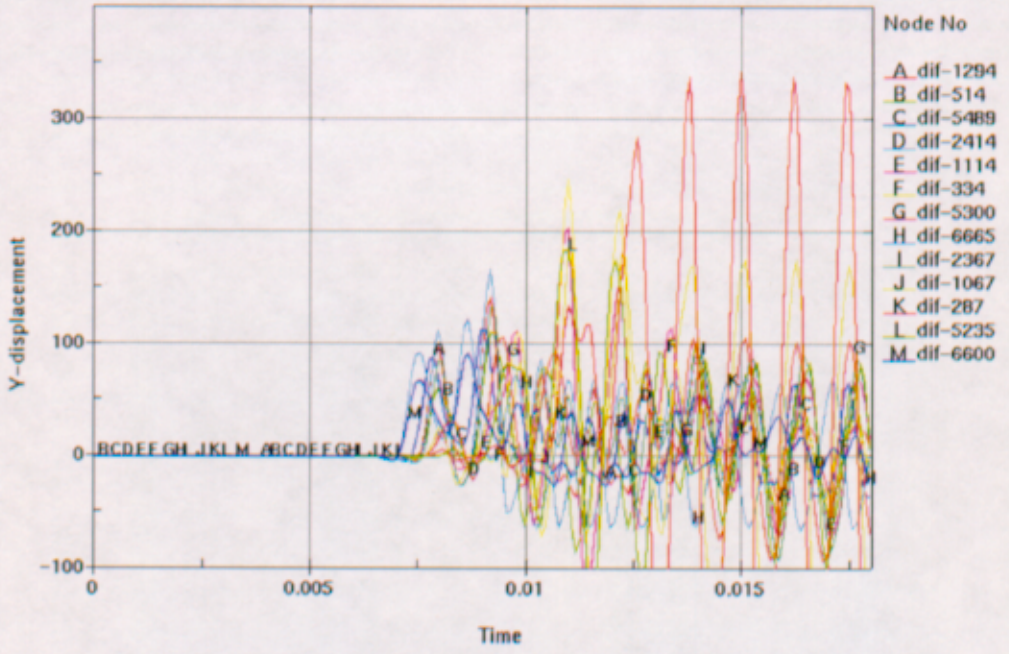

Figure V- 7. Accelerations plot (*g*), Initial Velocity = 1 *m/s*, T = 150 °C, Cutoff Frequency 1000 *Hz*

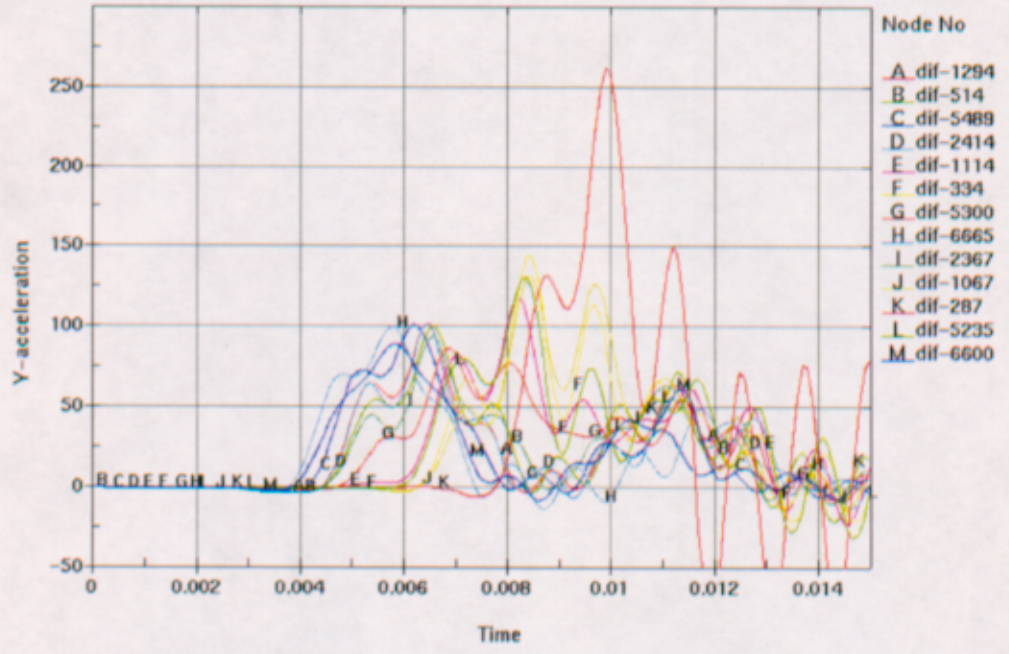

Figure V- 8. Accelerations plot (*g*), Initial Velocity = 2 *m/s*, T = 150 °C, Cutoff Frequency 450 *Hz*

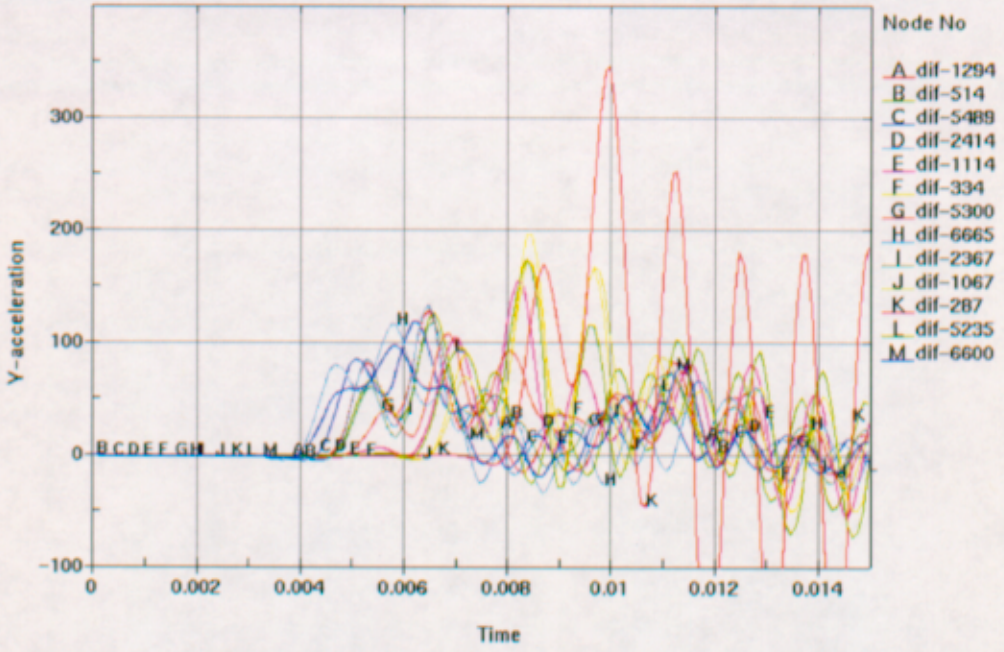

Figure V- 9. Accelerations plot (*g*), Initial Velocity = 2 *m/s*, T = 150 °C, Cutoff Frequency 600 *Hz*

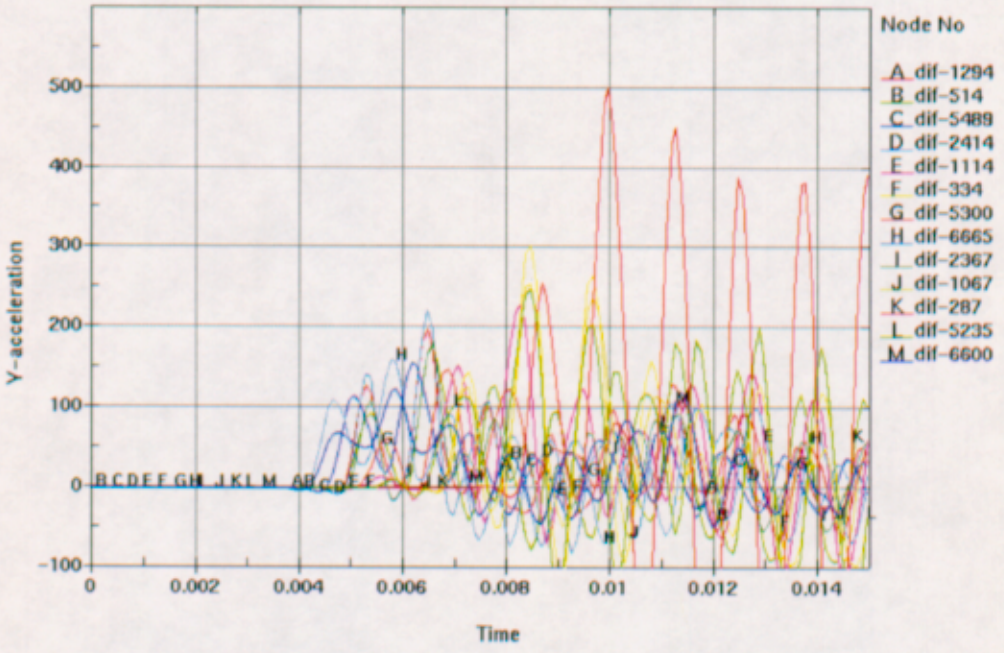

Figure V- 10. Accelerations plot (*g*), Initial Velocity = 2 *m/s*, T = 150 °C, Cutoff Frequency 1000 *Hz*

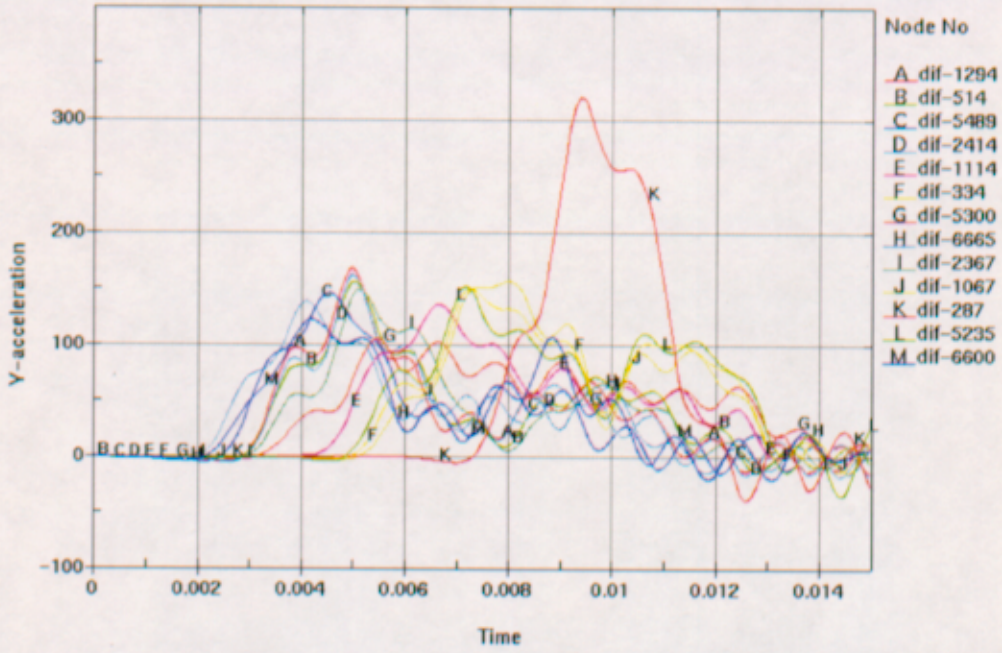

Figure V- 11. Accelerations plot (*g*), Initial Velocity = 4 *m/s*, T = 150 °C, Cutoff Frequency 450 *Hz*

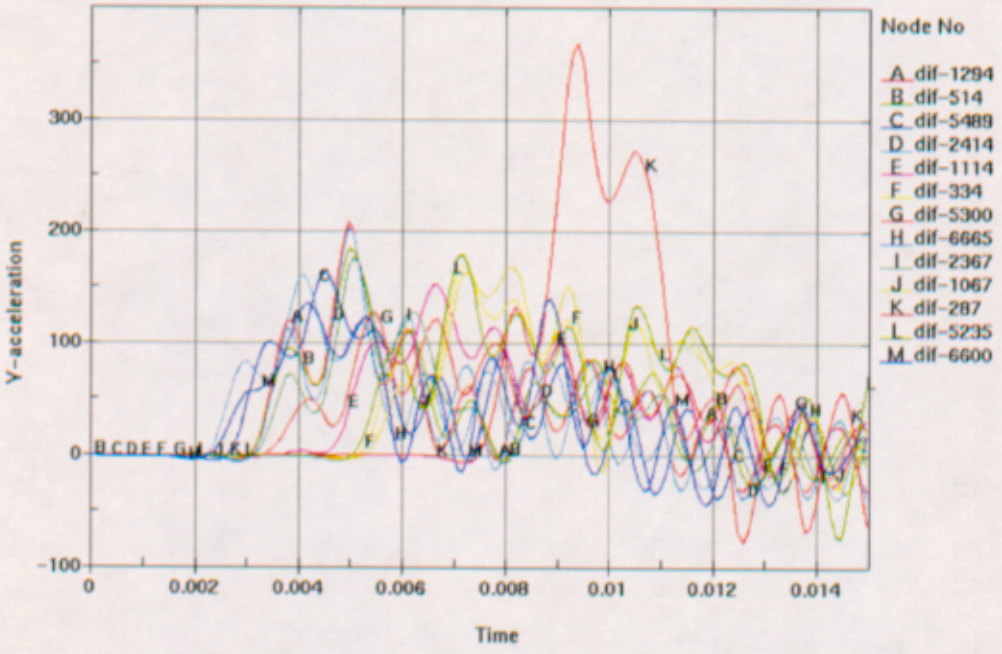

Figure V- 12. Accelerations plot (*g*), Initial Velocity = 4 *m/s*, T = 150 °C, Cutoff Frequency 600 *Hz*

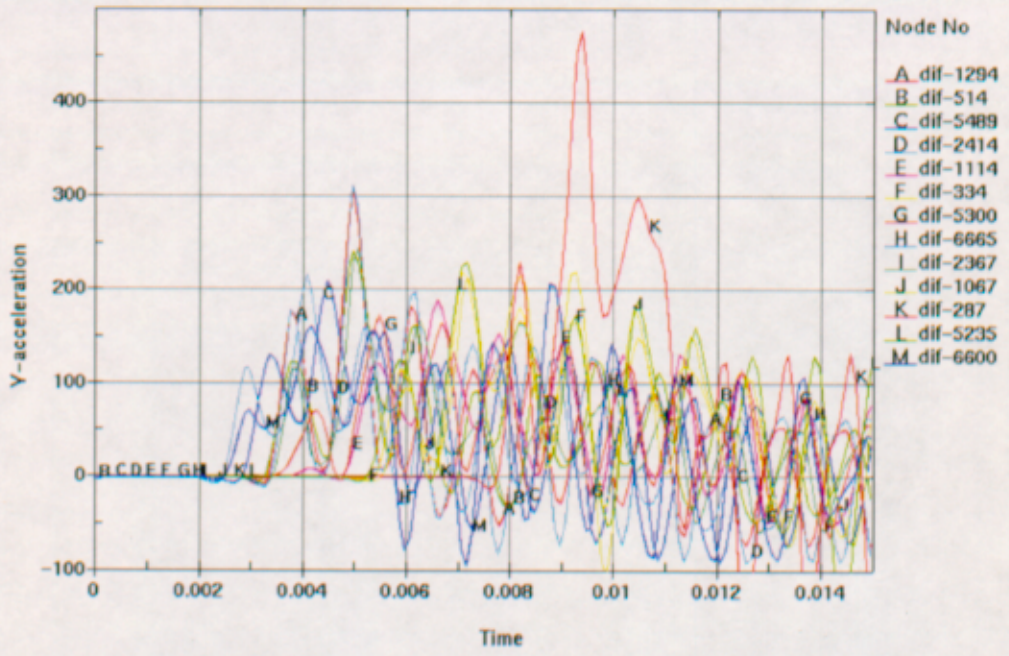

Figure V- 13. Accelerations plot (*g*), Initial Velocity = 4 *m/s*, T = 150 °C, Cutoff Frequency 1000 *Hz*

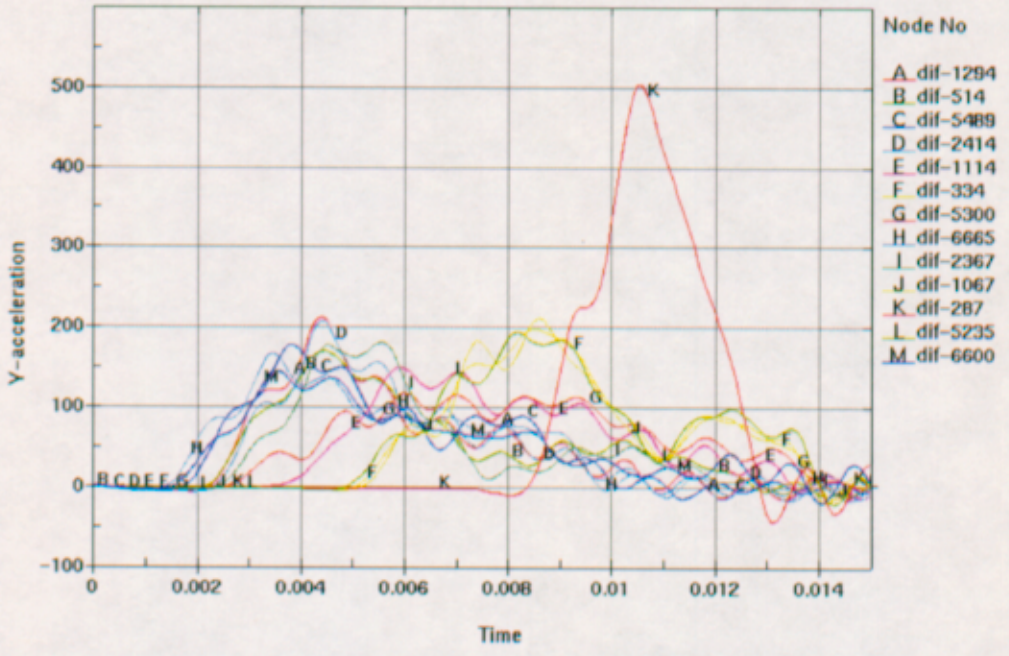

Figure V- 14. Accelerations plot (*g*), Initial Velocity = 6 *m/s*, T = 150 °C, Cutoff Frequency 450 *Hz*

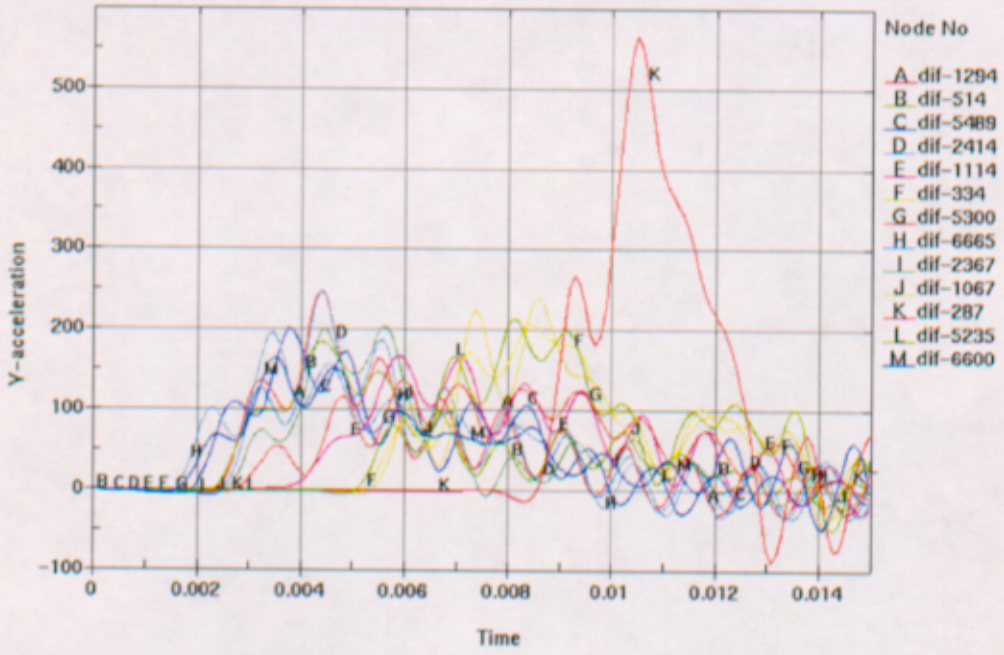

Figure V- 15. Accelerations plot (*g*), Initial Velocity = 6 *m/s*, T = 150 °C, Cutoff Frequency 600 *Hz*

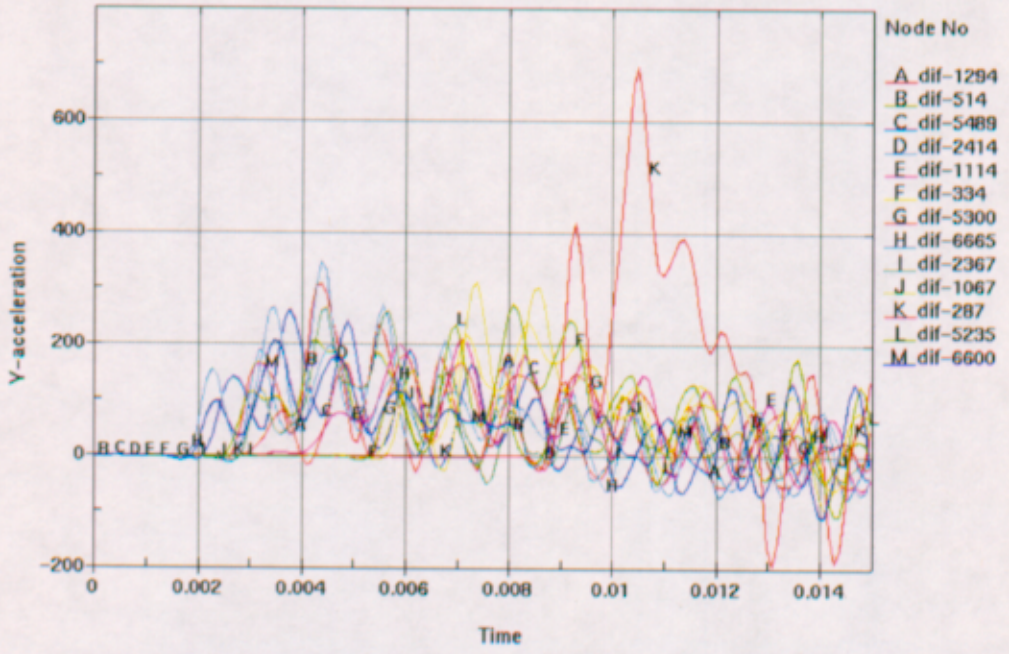

Figure V- 16. Accelerations plot (*g*), Initial Velocity = 6 *m/s*, T = 150 °C, Cutoff Frequency 1000 *Hz*

ATTACHMENT VI
EFFECT OF AMBIENT TEMPERATURE ON THE RESULTS

The object of this attachment is to present the results obtained for two simulations performed at an ambient temperature of 200 ℃, with initial velocities of 1 *m/s* and 4 *m/s*.

Tables VI- 1 and VI- 2 give the maximum accelerations obtained for the two temperatures, for an initial velocity of 1 *m/s*. Butterworth filtering is used with three different cutoff frequencies to remove the high-frequency response.

Table VI- 1. Maximum Accelerations (*g*) in three Fuel Assemblies for an Impact with Initial Velocity of 1 *m/s* at 150 ℃

	Cutoff Frequency (*Hz*)		
Fuel Assembly Number (See Figure II- 1)	**450 (See Figure VI- 1)**	**600 (See Figure VI- 2)**	**1000 (See Figure VI- 3)**
1 (node # 287)	144	192	343
2 (node # 1114)	74	114	204
3 (node # 5489)	62	75	113

Table VI- 2. Maximum Accelerations (*g*) in three Fuel Assemblies for an Impact with Initial Velocity of 1 *m/s* at 200 ℃

	Cutoff Frequency (*Hz*)		
Fuel Assembly Number (See Figure II- 1)	**450 (See Figure VI- 4)**	**600 (See Figure VI- 5)**	**1000 (See Figure VI- 6)**
1 (node # 287)	141	188	337
2 (node # 1114)	73	112	207
3 (node # 5489)	61	76	117

Table VI- 3 presents the relative difference of maximum acceleration between the two temperatures with an initial velocity of 1 *m/s*.

Table VI- 3. Comparison between the Results at two Different Temperatures for an Initial Velocity of 1 *m/s*

	Relative Difference in Acceleration (%), with Cutoff Frequency of		
Fuel Assembly Number (See Figure II- 1)	**450 *Hz***	**600 *Hz***	**1000 *Hz***
1 (node # 287)	-2.1	-2.1	-1.7
2 (node # 1114)	-1.4	-1.8	1.5
3 (node # 5489)	-1.6	1.3	3.5

Tables VI- 4 and VI- 5 give the maximum accelerations obtained for the two temperatures with an initial velocity of 4 *m/s*.

Table VI- 4. Maximum Accelerations (*g*) in three Fuel Assemblies for an Impact with Initial Velocity of 4 *m/s* at 150 °C

	Cutoff Frequency (*Hz*)		
Fuel Assembly Number (See Figure II- 1)	**450 (See Figure VI- 7)**	**600 (See Figure VI- 8)**	**1000 (See Figure VI- 9)**
1 (node # 287)	323	369	479
2 (node # 1114)	137	153	190
3 (node # 5489)	148	164	211

Table VI- 5. Maximum Accelerations (*g*) in three Fuel Assemblies for an Impact with Initial Velocity of 4 *m/s* at 200 °C

	Cutoff Frequency (*Hz*)		
Fuel Assembly Number (See Figure II- 1)	**450 (See Figure VI- 10**	**600 (See Figure VI- 11)**	**1000 (See Figure VI- 12)**
1 (node # 287)	307	346	433
2 (node # 1114)	128	140	172
3 (node # 5489)	143	155	206

Table VI- 6 presents the relative difference of maximum acceleration between the two temperatures with an initial velocity of 4 *m/s*.

Table VI- 6. Comparison between the Results at two Different Temperatures for an Initial Velocity of 4 *m/s*

	Relative Difference in Acceleration (%), with Cutoff Frequency of		
Fuel Assembly Number (See Figure II- 1)	**450 *Hz***	**600 *Hz***	**1000 *Hz***
1 (node # 287)	-5.0	-6.2	-9.6
2 (node # 1114)	-6.6	-8.5	-9.5
3 (node # 5489)	-2.7	-5.5	-2.4

The results obtained for two sets of simulations are in good agreement (relative difference under 10% for a temperature difference of 50 ℃). The change in temperature has minor effect on the results.

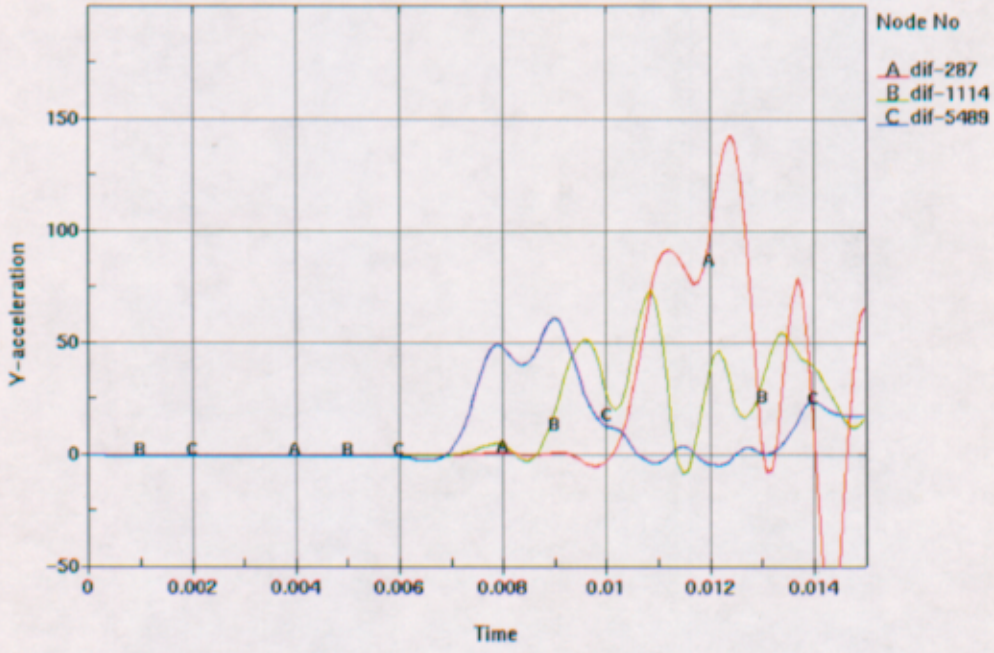

Figure VI- 1. Accelerations (*g*) for three Fuel Assemblies, Initial Velocity = 1 *m/s*, T = 150 ℃, Cutoff Frequency 450 *Hz*

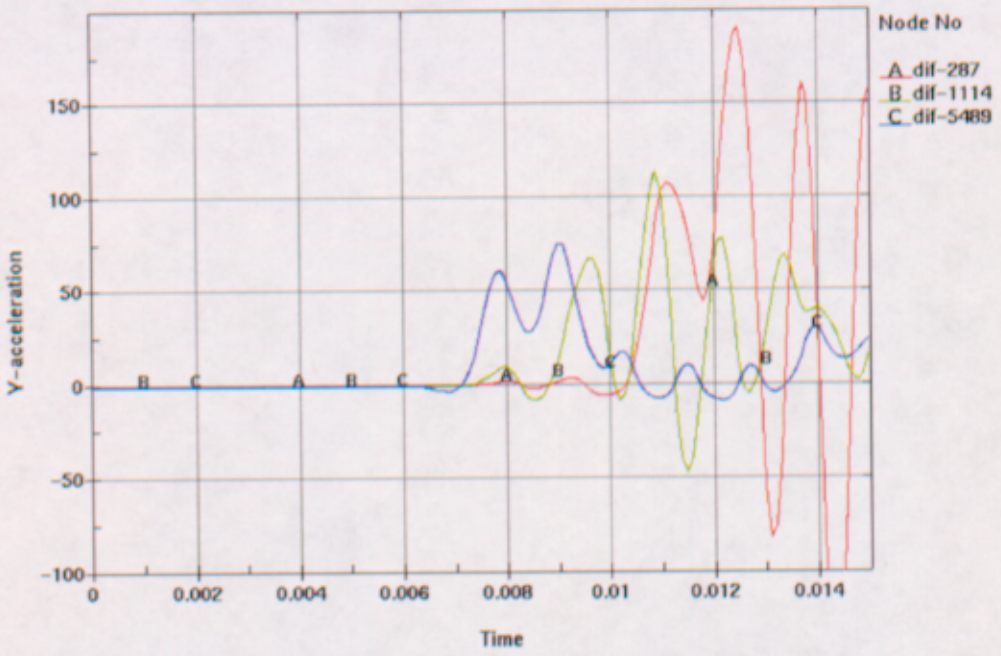

Figure VI- 2. Accelerations (*g*) for three Fuel Assemblies, Initial Velocity = 1 *m/s*, T = 150 °*C*, Cutoff Frequency 600 *Hz*

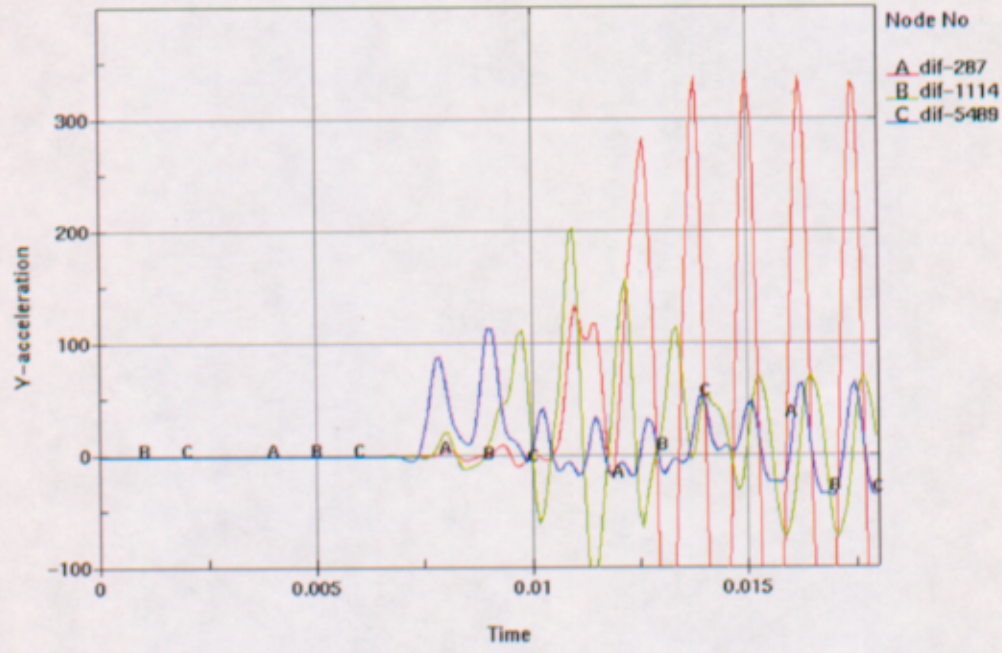

Figure VI- 3. Accelerations (*g*) for three Fuel Assemblies, Initial Velocity = 1 *m/s*, T = 150 °*C*, Cutoff Frequency 1000 *Hz*

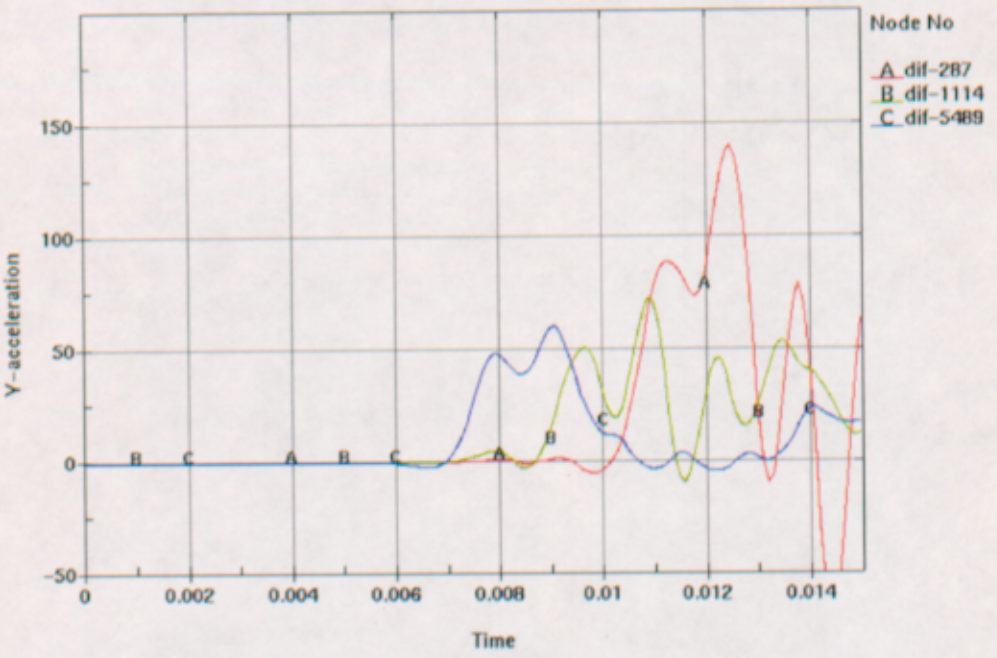

Figure VI- 4. Accelerations (*g*) for three Fuel Assemblies, Initial Velocity = 1 *m/s*, T = 200 °C, Cutoff Frequency 450 *Hz*

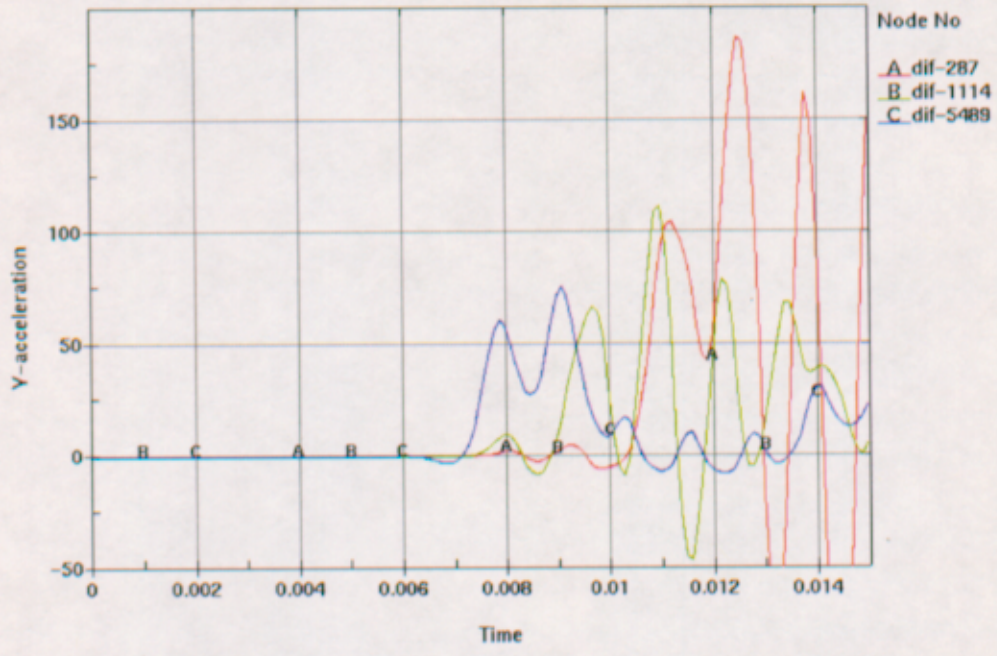

Figure VI- 5. Accelerations (*g*) for three Fuel Assemblies, Initial Velocity = 1 *m/s*, T = 200 °C, Cutoff Frequency 600 *Hz*

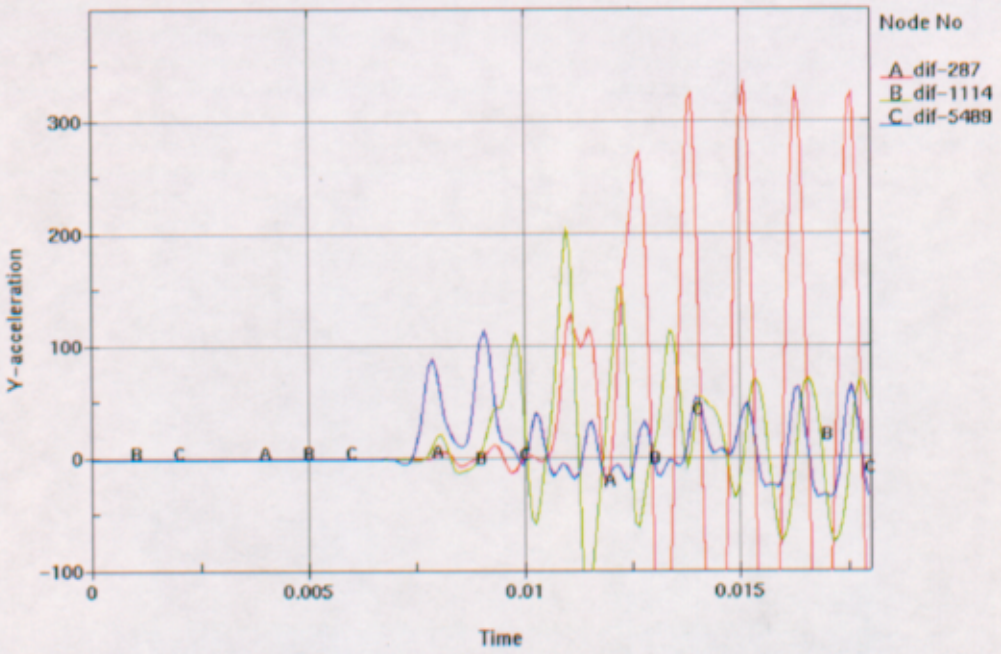

Figure VI- 6. Accelerations (*g*) for three Fuel Assemblies, Initial Velocity = 1 *m/s*, T = 200 *°C*, Cutoff Frequency 1000 *Hz*

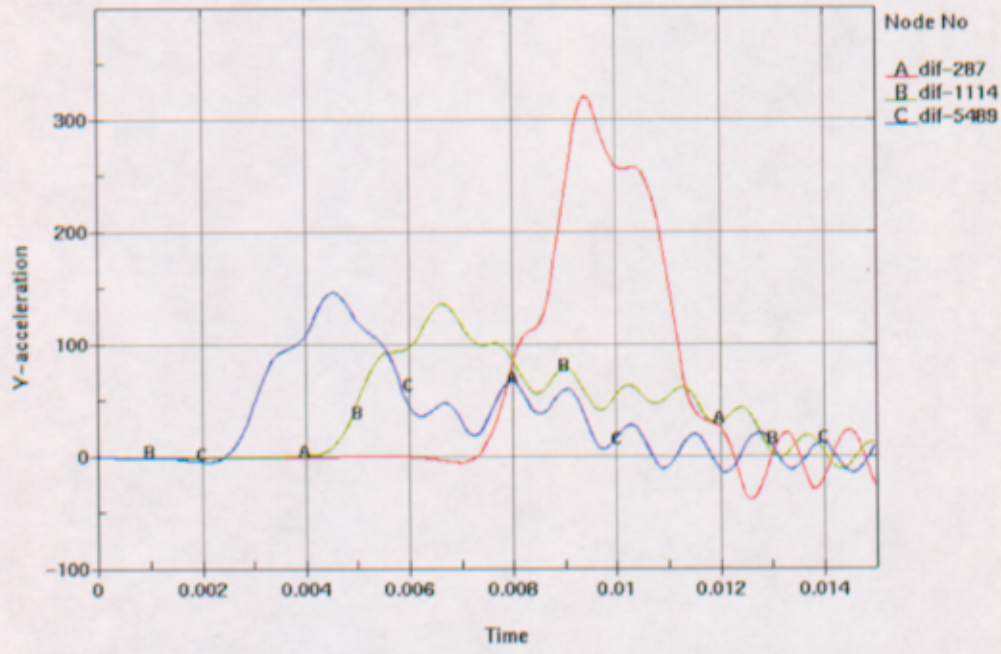

Figure VI- 7. Accelerations (*g*) for three Fuel Assemblies, Initial Velocity = 4 *m/s*, T = 150 *°C*, Cutoff Frequency 450 *Hz*

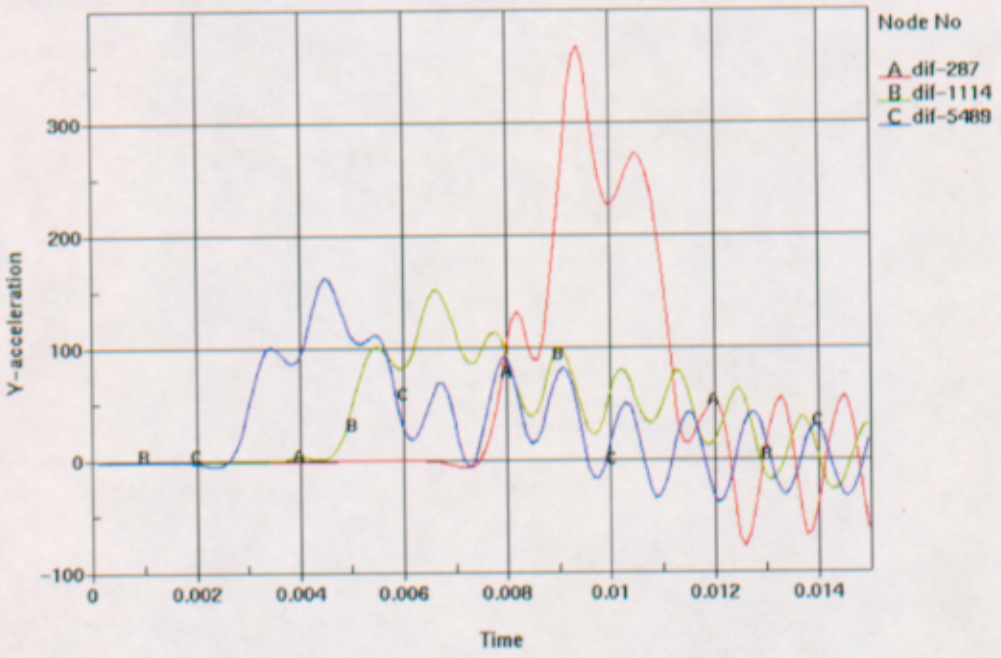

Figure VI- 8. Accelerations (*g*) for three Fuel Assemblies, Initial Velocity = 4 *m/s*, T = 150 °C, Cutoff Frequency 600 *Hz*

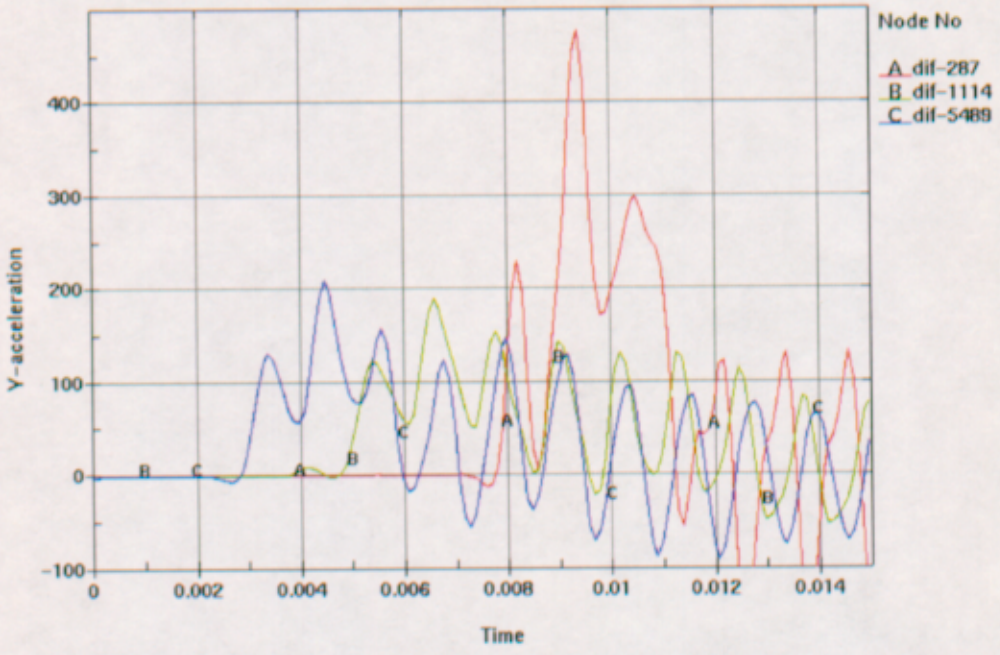

Figure VI- 9. Accelerations (*g*) for three Fuel Assemblies, Initial Velocity = 4 *m/s*, T = 150 °C, Cutoff Frequency 1000 *Hz*

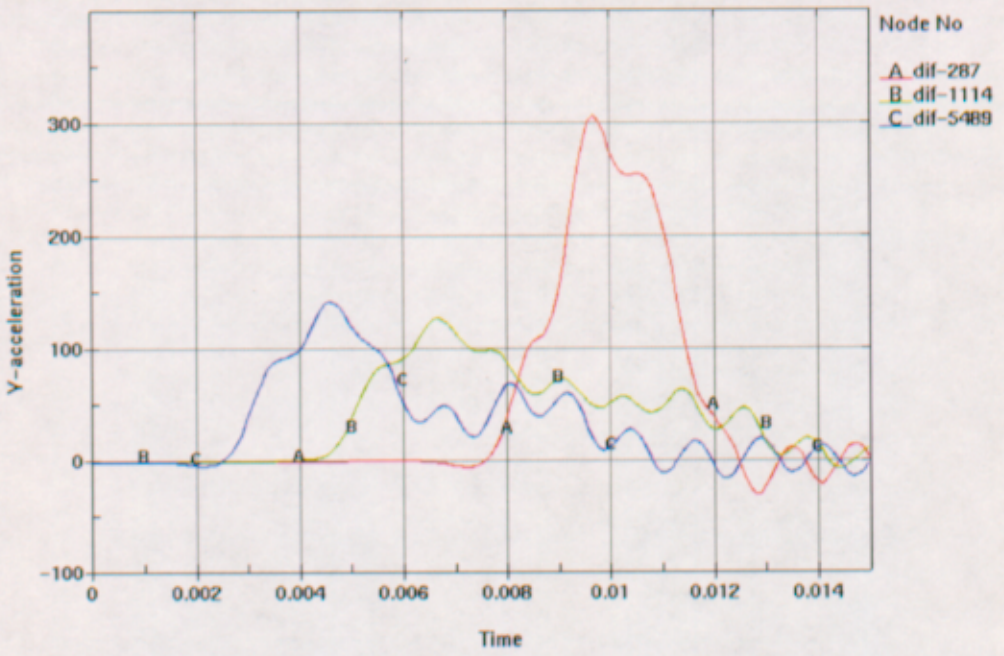

Figure VI- 10. Accelerations (*g*) for three Fuel Assemblies, Initial Velocity = 4 *m/s*, T = 200 °*C*, Cutoff Frequency 450 *Hz*

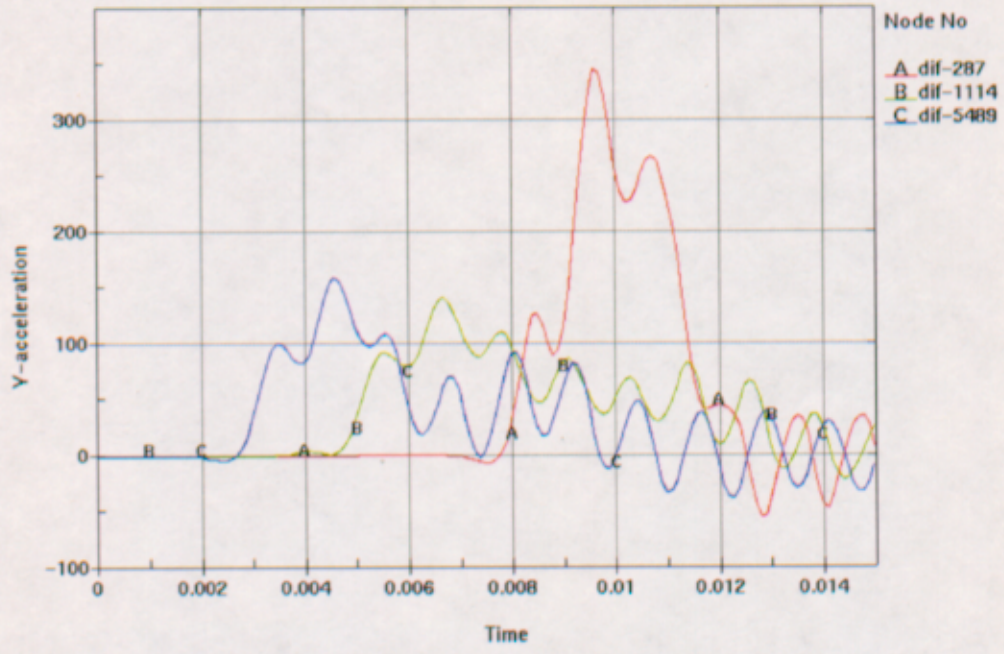

Figure VI- 11. Accelerations (*g*) for three Fuel Assemblies, Initial Velocity = 4 *m/s*, T = 200 °*C*, Cutoff Frequency 600 *Hz*

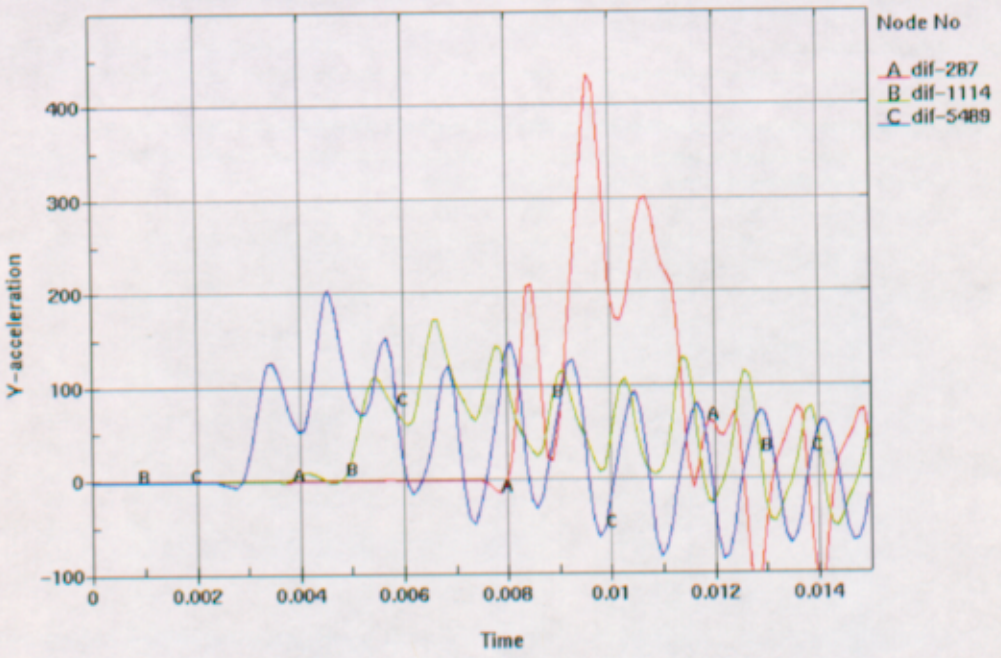

Figure VI- 12. Accelerations (*g*) for three Fuel Assemblies, Initial Velocity = 4 *m/s*, T = 200 *°C*, Cutoff Frequency 1000 *Hz*

ATTACHMENT VII
NATURAL FREQUENCIES OF THE FUEL ASSEMBLIES

This attachment presents the calculation of the first natural frequency for the fuel assemblies, for two configurations close to the geometry of the fuel assemblies in the waste package during the end impact.

1- First natural frequency for longitudinal vibrations of a fixed-free rod

According to Reference 17 (page 7.8), the first natural frequency for the longitudinal vibrations of a rod with one end fixed and one end free is

$$w_{1\,\text{fixed-free}} = \frac{\pi}{2L}\sqrt{\frac{Eg}{\gamma}}$$

where
L = length of the rod
E = Modulus of elasticity
γ = weight density of the fuel assemblies
g = acceleration of gravity

For the fuel assemblies, using the values given in Assumption 3.10 and Section 5.1.1 (at 150 ℃),

$$w_{1\,\text{fixed-free}} = \frac{\pi}{2\cdot 4.407}\sqrt{\frac{186\cdot 10^{9}\cdot 9.81}{9.81\cdot\frac{773.4}{4.407\cdot 0.217^{2}}}} = 2518\ \text{rad/s} = 401\ \text{Hz}$$

2- First natural frequency for longitudinal vibrations of a free-free rod

Similarly, using the general equation of motion for an element of a rod given in Reference 17 (Equation 7.7) and the boundary conditions corresponding to both ends of the rod being free, one can readily obtain the first natural frequency for the longitudinal vibrations of a free-free rod:

$$w_{1\,\text{free-free}} = \frac{\pi}{L}\sqrt{\frac{Eg}{\gamma}}$$

Thus, for the fuel assemblies, $w_{1\,\text{free-free}} = 5036\ \text{rad/s} = 802\ \text{Hz}$.

Therefore, three values of cutoff frequencies are used to postprocess the results throughout this document: 450 *Hz*, 600 *Hz* and 1000 *Hz*.